Research Square

Preprints are preliminary reports that have not undergone peer review.
They should not be considered conclusive, used to inform clinical practice,
or referenced by the media as validated information.

The Antibody Dependant Neurite Outgrowth Modulation Response (ADNM) involvement in Spinal Cord Injury

Alice Capuz
Unversité de Lille, INserm, CHU Lille
Mélodie-Anne karnoub
Unversité de Lille, INserm, CHU Lille
Sylvain Osien
Unversité de Lille, INserm, CHU Lille
Melanie Rose
University of Lille https://orcid.org/0000-0002-2043-4856
Céline meriaux
Unversité de Lille, INserm, CHU Lille
Isabelle Fournier
Unversité de Lille, INserm, CHU Lille https://orcid.org/0000-0003-1096-5044
David devos
Université de Lille, INSERM, CHU-Lille
Fabien Vanden Abeele
Inserm U-1003, Equipe labellisée par la Ligue Nationale contre le cancer, Laboratory of Excellence, Ion Channels Science and Therapeutics, Université Lille 1, Cité Scientifique, 5
Franck Rodet
University of Lille https://orcid.org/0000-0002-7612-0282
Dasa Cizkova
Institute of Neurobiology, Slovak Academy of Sciences https://orcid.org/0000-0002-2504-3993
Michel salzet (michel.salzet@univ-lille.fr)
Unversité de Lille, INserm, CHU Lille https://orcid.org/0000-0003-4318-0817

Article

Keywords: Spinal Cord Lesion, Proteomic, IgG, Acute Phase, Inflammation, Astrocytes, Shot Gun Proteomic, Neurite outgrowth, ADNM, Autoantibodies, Shot gun proteomic, Spinal Cord Injury

Posted Date: February 11th, 2022

DOI: https://doi.org/10.21203/rs.3.rs-1349635/v1

License: This work is licensed under a Creative Commons Attribution 4.0 International License.
Read Full License

Abstract

Spinal Cord Injury (SCI) represents a major medical challenge. At present, there is still no cure to treat it efficiently and enable functional recovery at the level of cavity. Previously, we demonstrated that inflammation determine the fate of the physiopathology. In an attempt to decipher the molecular mechanisms involved in this process, we performed a meta-analysis of our spatio-temporal proteomic studies in time course of SCI. This highlighted the presence of IgG isotypes in both the tissues and secretome of spinal cord explants. These IgGs which were detected even if no SCI occurs in spinal cord, followed the time course and the spatial repartition with presence of IgG1 and IgG2 subclasses (a, b, c). IgG1 was clearly mostly abundant at 12h and switch in time course to IgG2a at 24h then stay predominant 3, 7 and 10 days after SCI. A protein related to IgM as well as a variable heavy chain were detected only 12h after lesion. Interestingly, RhoA inhibitor treatment influences the IgG isotypes switching preferentially to IgG2c. By transcriptomic analyses using data reuse of rat dorsal root ganglion (DRG) neurons RNAseq datasets and RT-PCR experiments performed on cDNA from DRG sensory neurons (ND7/23 and dopaminergic neurons N27 cell lines), we confirmed expression of immunoglobulin heavy and light chains (constant and variable) encoding genes in neurons. We then identified CD16 and CD32b as their specific receptors in sensory neuron cell line ND7/23 and regulate neurites outgrowth. Therefore, we propose a new view of the spinal cord injury response involving an antibody dependent neurite outgrowth modulation (ADNM) which could be precursor of the neuroinflammatory response in pathological conditions.

Introduction

Spinal cord represents, with the brain, one the two parts of central nervous system (CNS). It supports all nerves, coming from or going to the peripheric nervous system. It is protected by the spinal canal, formed by the articulation of cervical, thoracic and lumbar vertebrae. This is why vertebral fracture or luxation can lead to spinal cord injury (SCI), from concussion/contusion to section[1]. The clinical consequences of these lesions are terrible, for they lead, according to the level, either to paraplegia or tetraplegia, which can be complete or incomplete. According to the literature, the incidence ranges between 19.4 patients per year and million inhabitants in Europe, and 51 patients per year and million inhabitants in Northern America [2]. This represents not only an epidemiologic, but also a social and economic burden, because of the population affected, represented by young men with a mean age of 40 years old. The SCI etiologies gather car crash (31.47%), falls (25.29%), gunshot wounds (10.42%), motorcycle crash (6.80%) and diving (4.67%) [2].

Although fundamental understanding has been obtained through various modeling studies, there is still a lack of knowledge about the pathophysiology of SCI, but all starts with a primary mechanic traumatism by compression, laceration, distraction or shearing [3]. This induces vascular lesions that lead to the formation of a hematoma on the lesion site, which itself causes a local ischemia, edema, and cell regulated cell death such apopotosis [3]. Moreover, the blood spinal cord barrier is disrupted, which initiates

the secondary extension of the lesion by the attraction of inflammatory cells, the accumulation of cytokines and vasoactive proteins. Finally, cell death is responsible of accumulation of cellular debris, potassium, ATP, leading to a cytotoxic environment. Then attracting pro-inflammatory M1 microglial cells and phagocytes infiltrate this cytotoxic environment leading to an oxidative stress which is toxic to adjacent neurons [3]. In our laboratory, a previous study, focused on subacute inflammatory response after SCI demonstrated that after 3 days, inflammatory response is intense in lesion and in downstream caudal 1 segment, where high amounts of cytokines and immunoglobulins are detected, and where the Rho-Rock and Memo1-RhoA-Diaph1 pathways are activated [4, 5].On the contrary, more caudally and distally from the central lesion, we have rather detected neurite outgrowth proteins and chemokines attracting first neutrophils, then T regulatory cells, anti-inflammatory M2 microglial cells, leading to creating a beneficial environment possibilities for neurite outgrowth on both sides of the lesion [4].

Several currently tested innovative treatments inhibit ligands known to engage the Rho-Rock pathway in neurons. These notably include Chondroitin Sulfate Proteoglycans, Myelin Associated Glycoprotein (MAG), Oligodendrocyte Myelin Glycoprotein (OMGP) and Neurite Outgrowth inhibitor A (NOGO-A). For examples, anti-NOGO-A antibodies delivered in the cerebrospinal fluid have been used in a phase I clinical trial [6, 7], with promising results. Also, in pre-clinical studies, chondroitinase ABC was shown to partially block the Rho-Rock-mediated inhibition of neurite outgrowth and glial scar formation within the lesion [8]. Finally, a RhoA inhibitor (RhoAi), called Cethrin [9, 10], has been assessed in both a phase I and a phase IIa clinical trial on patients suffering from cervical SCI, with an increase of functional repair [11]. A phase IIb is foreseen. However, we recently shown that 12h after lesion, the mechanism which are occurring are completely different to the ones from after 1 day. At 12h after SCI, rostral and caudal segments are not molecularly different except the lesion [12]. Repetitive delivery of RhoA inhibitor significantly increases the synaptogenesis and help to stimulate neuritogenesis and neurite outgrowth through the cavity [12]. However, a week after lesion a plateau appears which blocks the achievement of the biological processes and the neuronal reconnection. Among the proteins which can be evoked to participate to such inhibition we initially observed in SCI secretome that IgG1 and IgG2 isotypes were already present 12 hours after lesion [4, 12]Then, we confirmed their presence in astrocytes even after a preventive treatment with anti-CD20 24h after SCI [4, 12]In this context, we investigated the identification of such immunoglobulins in time course after SCI from 12h to 7 days. A meta-analysis was performed with MaxQuant software, in two rows. First analysis was performed against the SCI data [4] at several times (12h, 1 day, 3 days, 7 days and 10 days), and with several segments including rostral (R3, R2, R1), lesion (L) and caudal (C1, C2, C3). We then investigate their expression and the ones of their specific receptors in neurons and their activity linked to neurites outgrowth.

Materials And Methods

Reagents

All chemicals were obtained with the highest purity available. Water, acetonitrile (ACN), formic acid (FA), trifluoroacetic acid (TFA), were purchased from Biosolve B.V. (Valkenswaard, The Netherlands). DL-dithiothreitol (DTT), HEPES, ES FBS, thiourea, iodoacetamide (IAA), Tri-reagent, isopropanol, chloroform, glucose and agarose were purchased from Sigma Aldrich. Lys-C/Trypsin enzymatic mixture, DNase RQ1, deoxyribonucleotides (dNTPs), RNAsin® ribonuclease inhibitor, RNase H, GoTaq® G2 Hot Start Taq polymerase kit, molecular weight markers, PGEM-T Easy Vector System II®, T4 DNA ligase and *E. coli* strain JM109 were purchased from Promega (France). Random primers, Superscript® III kit, phosphate buffered saline (PBS), Dulbecco's modified Eagle's medium (DMEM), RPMI 16140, fetal bovine serum (FBS), L-glutamine, penicillin and streptomycin, the GeneJET Gel Extraction kit, Alexa Fluor® 647-conjugated goat anti-rat IgG, Alexa Fluor® 488-conjugated donkey anti-rabbit, Alexa Fluor® 488-conjugated donkey anti-mouse, melon Gel IgG Spin Purification Kit and Zeba Spin Desalting Columns (7K MWCO), Dynabeads Protein G and enhanced chemiluminescence kit were obtained from Life Technologies (Milan, Italy). RhoA inhibitor was obtained from Cytoskeleton, Inc. (Denver, Co). All primers used were purchased from Eurogentec. The QiAquick PCR Purification kit was purchased from Qiagen®. The NucleoSpin® Plasmid kit was purchased from Macherey Nagel. Urea was purchased from Euromedex.Mouse anti-GFAP, mouse anti-NeuN, Amicon ultracentrifugal filter 10K and ZipTip C18 were purchased from Millipore. Mouse anti-CD16 and rabbit anti-CD32 were obtained from Santa Cruz Biotechnology. Peroxidase-conjugated goat anti-rat IgG is from Thermofisher scientific, peroxidase-conjugated goat anti-mouse IgG and peroxidase-conjugated goat anti-rabbit IgG were obtained from Jackson ImmunoResearch (West Grove, PA, USA). Ultrapure Lipopolysaccharides (LPS-EB) were bought from InvivoGen (Toulouse, France). PNGase F was bought from New Englands Biolabs (USA).

Secretome preparation

All studies were carried out on adult male Wistar rats with the agreement and according to the rules laid down by the institutional committee for the protection of animals of the Slovak University of Science and by the European Directive 2010/63 on the use of the animals for research purposes, as well as with the Slovak animal welfare laws Nos. 377/2012 and 436/2012. Some of the animals underwent spinal cord injury at Th8-Th9 level by the balloon compression method, performed after laminectomy. Other animals, called "control" did not undergo compression but a simple laminectomy. Some have also received treatment with RhoA inhibitor, injected at lesion site at time of lesion. Rats were sacrificed after isoflurane anesthesia, 12 hours (12h) (3 rats not treated with RhoA inhibitor and 3 rats treated with RhoA inhibitor) or 24 hours (24h) (5 rats) after injury. Spinal cords were extracted by injection of sterile saline buffer and divided into 1 cm long segments, on both sides of lesion, which level was macroscopically verified, making it possible to obtain a lesion segment, 2 rostral segments and 2 caudal segments, each segment being cut into two fragments of 0.5 cm. These fragments were then cultured for 12 hours and 24 hours in DMEM at 37°C and 5% CO2, and conditioned medium thus obtained was called secretome.

Preparation of intact spinal cord

Rats were sacrificed after isoflurane anesthesia. Spinal cord was extracted by injection of sterile saline buffer and immediately frozen as a whole.

Cell line

The rat dorsal root ganglion (DRG) cell line ND7/23 and N27 dopaminergic cell line were purchased from Sigma-Aldrich. ND7/23 cells were obtained by PEG mediated cell fusion between the mouse neuroblastoma (N18 tg 2) and the rat dorsal root ganglion neurons. ND7/23 cell line was grown in DMEM medium supplemented with 10% fetal bovine serum, 1% L-glutamate, 100 U/ml penicillin and 100 µg/ml streptomycin, at 37°C in a humidified atmosphere (5% CO2). N27 cells were cultivated in RPMI 1610 supplemented with 10% embryonic FBS, 1% L-glutamate, 100 U/ml penicillin and 100 µg/ml streptomycin, at 37°C in a humidified atmosphere (5% CO2).

Protein Extraction

To extract the proteins, ND7/23 3DRG cells were resuspended in RIPA buffer (150 mM NaCl, 50 mM Tris, 5 mM EGTA, 2 mM EDTA, 100 mM NaF, 10 mM sodium pyrophosphate, 1% Nonidet P-40, 1 mM PMSF, 1X protease inhibitors) and subjected to three sonications of 5 seconds with a step on ice for 30 seconds between the sonications. Then the samples were centrifuged at 14,000 x g for 20 minutes at 4°C. The supernatant containing the proteins was collected. To determine protein concentration in the samples, Bradford assay was used.

As a first step to purify antibodies from spinal cord lesion segment withdrawn seven days after injury (SCI 7D-L), proteins were extracted from 50 mg of tissue resuspended in RIPA buffer and submitted to the same procedure as described above. Seven days were chosen to mimic the dynamic of the inflammatory response that occurs 7 days after lesion.

To conduct shotgun proteomics analysis on non-injured spinal cords, control spinal cords as well as on rostral, lesion and caudal spinal cord segments collected 12h after SCI, protein extraction was performed as follow. Tissues were cut to obtain small fragments of 1 mm thick and grinded in liquid nitrogen. Powders were resuspended in CHAPS lysis buffer (CHAPS 3.5%, Tris-HCl and DTT, pH 10), mixed thoroughly and subjected to sonication during 20 minutes. Samples were heated at 95°c during 5 minutes and centrifuged at 15,000 x g during 5min at 4°C. Supernatants containing proteins were then collected.

Enrichment procedure for immunoglobulins from SCI 7D-L protein extracts.

To purify antibodies from protein extracts of SCI 7D-L obtained after RIPA extraction, ammonium sulfate precipitation was carried out on 500 µg of proteins according to the protocol in the Melon Gel IgG Purification Kit, with a few modifications. Briefly, saturated ammonium sulfate solution was prepared by dissolving 7.61 g ammonium sulfate in 10 mL milliQ water. Then, after measuring the volume of the sample, an equal volume of saturated ammonium sulfate solution was added in order to have 50% ammonium sulfate. Sample was incubated during 4 hours at 4°C, and centrifuged at 3,000 x g for 20

minutes at 4°C. The supernatant was then removed and the pellet was resuspended in a volume of milliQ water, equivalent to the original volume of the sample. The resuspended pellet containing the purified antibodies was desalted thanks to the Zeba Spin Desalting Columns according to manufacturer's instructions. Column's caps were removed and column was placed in a 2.0 mL collection tube, prior to centrifugation at 1,500 x g for 1 minute in order to remove the storage solution. Wash was performed by adding 300 µL of milliQ water to the column, and centrifugation at 1,500 x g for 1 minute. Wash process was repeated two more times. Ensuing these steps, sample was carefully added to the center of the column, and centrifuged at 1,500 x g for 2 minutes in order to collect the desalted sample. Melon Gel IgG Purification was then assessed according to manufacturer's instructions. Purification Buffer and Melon Gel IgG Purification Support were equilibrated for 15 minutes at room temperature. During this time, sample was completed to 500 µL with Purification Buffer. Then, after swirling the bottle containing the gel, 500 µL of slurry were dispensed into a Spin Column placed in a microcentrifuge tube, and centrifuged for 1 minute at 4,000 x g. The flow-through was discarded afterwards, and two washes were performed by adding 300 µL of Purification Buffer and quickly centrifuged at 4,000 x g for 10 seconds. The flow-through was discarded again, and the sample were loaded to the column. The column was capped and mixed end-over-end for 5 minutes at room temperature, in order to let the nonspecific proteins bind to the resin. Bottom cap was removed, top cap was loosed, and centrifugation was performed at 4,000 x g for 1 minute to collect the purified antibodies in a new collection tube. After the Melon Gel Purification, samples were digested after reduction, alkylation and deglycosylation.

Reduction, Alkylation, Deglycosylation and Trypsic Digestion of samples obtained after Melon Gel IgG Purification

Reduction was performed by the addition of DTT 200 mM to the sample, in order to have a final concentration of 50 mM, and sample was incubated at 56°C for 1 hour. Then, sample was loaded into an Amicon 10K to change the buffer and retain the proteins on the membrane. To do that, around 450 µL was loaded into the column, centrifugation at 14,000 x g was done for 15 minutes, and flow-through was discarded. This step was performed four times in order to load the entire sample, due to the maximum capacity of the Amicon which is 500 µL. Then washes step were performed by the addition of 200 µL NH_4HCO_3 50 mM to the column, centrifugation at 14,000 x g for 15 minutes, and flow-through removal. After these steps, around 40 µL of the sample should remain in the Amicon 10KAlkylation was then performed by the addition of 100 µL IAA 50 mM, mixed briefly at 600 RPM, and incubated in the dark for 20 minutes. Then centrifugation was performed at 14,000 x g for 15 minutes, and two washes was performed by the addition of 200 µL NH_4HCO_3 50 mM, centrifuged at 14,000 x g for 15 minutes, and flow-through removal. Ensuing these steps, deglycosylation with PNGase F was carried out. PNGase F was prepared with NH_4HCO_3 50 mM (1:99, v/v), and a volume of this solution was added to the sample in order to have 10% of diluted PNGase F in the final sample. Then, sample was mixed briefly at 600 RPM and incubated overnight at 37°C. The next day, two washes were performed by the addition of 200 µL NH_4HCO_3 50 mM to the column, centrifuged at 14,000 x g for 15 minutes, and flow-through removal.40 µL Trypsin (20 ng/µL in NH_4HCO_3 50 mM) was added to the sample which was mixed briefly at 600 RPM,

and incubated overnight at 37°C. The addition of trypsin quenched the reaction with PNGase F. The next day, new collection tube was placed and 40 µL NH_4HCO_3 50 mM was added to the column, then centrifugation was performed at 14000 x g for 10 minutes to collect the digested sample. Trypsin digestion was then quenched by the addition of TFA at a final concentration of 1%. Finally, sample was dried in the SpeedVac and desalted with ZipTip C18 before HPLC-MS/MS analysis.

Reduction, Alkylation and Trypsic Digestion of secretomes from spinal cord segments collected 12h (treated or not with RhoA inhibitor) and 24h after SCI.

Secretomes were deposited on 0.22 µm syringe filters. After filtration, denaturation of the proteins contained in the secretomes was performed with Urea 6M and HEPES 40 mM. Reduction was then carried out by DTT at a final concentration of 10 mM. at 56°c during 40 min. Afterwards, alkylation was conducted with IAA 55 mM 40min at room temperature and obscurity. Thiourea 100 mM was added to stop the reaction and digestion was performed overnight at 37°C with Lys-C/Trypsine (30µg/mL). Addition of TFA 0.5% stopped the reaction. Finally, samples were dried in the SpeedVac and desalted with ZipTip C18 before HPLC-MS/MS analysis.

Reduction, Alkylation and Trypsic Digestion of protein extracts from non-injured spinal cords, control spinal cords as well as on rostral, lesion and caudal spinal cord segments collected 12h after SCI

Thirty microliters of each sample were loaded into an Amicon 30K and 200 µL of UA buffer (Urea 8 M, Tris-HCl 0.1 M pH 8.5) were added. Samples were centrifuged at 14,000 x g during 15 minutes and flow-through was discarded. Alkylation was conducted with 100 µL of IAA 55 mM, UA buffer was then added and samples were centrifuged at 14,000 x g during 15 minutes. This step was repeated three times. Ammonium Bicarbonate (AB) buffer was then added and samples were centrifuged three times at 14,000 x g during 15 minutes. Digestion was performed overnight at 37°C with Lys-C/Trypsine (30µg/mL). After centrifugation at 14,000 x g for 10 minutes, 500µL of NaCl and TFA 0.5% were added. Finally, samples were dried in the SpeedVac and desalted with ZipTip C18 before HPLC-MS/MS analysis.

SDS-PAGE and in gel digestion

To identify immunoglobulins in secretomes of segments R1, L and C1 of 12 h and 24h post SCI, 2.5 µg of proteins of each sample were separated on a 12% SDS-polyacrylamide gel (SDS-PAGE). Gels were colored overnight at room temperature with Coomassie blue and eventually in gel digestion was carried out. Bands of interest were cut in small pieces of approximately 1 mm square and placed in new microtubes. 300 µL milliQ water were added to the gels pieces and mixed for 15 minutes, then 300 µL ACN were also added and mixed for 15 minutes. The supernatant was removed afterwards, and 300 µL NH_4HCO_3 100 mM were put with the gel pieces, followed by 15 minutes mixing and supernatant removing. 300 µL of ACN/ NH_4HCO_3 100 mM (1/1, v/v) were added, 15 minutes mixing was performed and supernatant was discarded. As a final wash, 100 µL ACN were added to the gel pieces and 10 minutes mixing was carried out. Band pieces should become white and shrinked, then ACN was removed and band pieces were dried in the SpeedVac for 10 minutes. Reduction was performed on the band

pieces by the addition of 50 µL/band DTT 10 mM in NH_4HCO_3 100 mM, and incubation at 56°C for 1 hour. Following this step, 50 µL/band IAA 50 mM in NH_4HCO_3 100 mM were added to the gel pieces and sample was incubated for 30 minutes in the dark, at room temperature. Then supernatant was removed and 300 µL NH_4HCO_3 100 mM were added and mixed for 15 minutes. Supernatant was removed again, and 300 µL ACN/ NH_4HCO_3 20 mM (1/1, v/v) were put with the band pieces and mixed for 15 minutes. Ensuing this mixing, supernatant was removed and a final wash with 100 µL ACN was performed with mixing for 10 minutes. Band pieces should become white and shrinked, and ACN was removed from the sample which was dried for 10 minutes in the SpeedVac. Digestion was then performed. 50 µL Trypsin (20 ng/µL) were added to the band pieces, and incubation at 37°C was performed overnight. The next day, 50 µL ACN were added to the sample and again incubated at 37°C for 30 minutes, followed by mixing for 20 minutes. The supernatant containing the peptides was transferred afterwards to a new microtube. 50 µL of 1% FA were added to the band pieces which were mixed for 20 minutes, and the supernatant was collected in the new tube from the previous step. This last step was carried out four times in total. Afterwards 150 µL ACN were added to the band pieces, mixed for 10 minutes. The supernatant was collected again and added to the tube containing peptides. The peptides were finally dried in the SpeedVac and desalted with ZipTip C18 prior to HPLC-MS/MS analysis.

HPLC-MS/MS

An online reversed-phase chromatography is used to separate the sample, through a Thermo Scientific Proxeon easy nLC1000 equipped with a Proxeon trap column (100 µm ID x 2 cm, Thermo Scientific) and a C18 packed-tip column (Acclaim PepMap, 75 µm ID x 15 cm, Thermo Scientific). Peptides were separated with an increasing amount of ACN (2%-40% over 60 minutes) at a flow rate of 300 nL/min. The peptides were electrosprayed directly from the analytical column and a voltage of 1.7 kV was applied via the liquid junction of the nanospray source. The chromatography system was coupled to the mass spectrometer Thermo Scientific Q- exactive programmed with a top 10 data-dependent mode for all the samples. The resolving power was 70,000 FWHM (m/z 400), in a positive mode and using an AGC target of 3e6. Default charge state was set at 2, unassigned and + 1 charge states were rejected and dynamic exclusion was enabled for 25s. The scan range was set to 300–1600 m/z. For ddMS², the scan range was between 200–2000 m/z, 1 microscan was acquired at 17,500 FWHM and an isolation window of 4.0 m/z was used.

MS Data analysis

The MS data from secretome were analyzed through MaxQuant 1.6.2.6 using the Andromeda search engine. Proteins and peptides were searched against a custom databank composed of the complete proteome of Rattus norvegicus (29961 entries, July 2018) from the Uniprot database. Carbamidomethylation was set as a static modification, and Methionine Oxydation was set as a variable modification. Moreover, due to the deglycosylation, asparagine to aspartate was set also as a variable modification only for samples subjected to the deglycosylation. Parameters were set to 1 peptide per protein, 2 miss cleavages, with a strict FDR of 0.01. The mass tolerance was 10 ppm for the precursors,

and 0.6 ppm for the fragments. Relative, label free quantification was performed using the MaxLFQ algorithm integrated in MaxQuant software, with the default parameters. LFQ intensity was logarithmized (log2[x]). Proteins only identified with modified peptides and potential contaminants were removed The MS data from astrocytes samples were analyzed through Proteome Discoverer 2.2. Proteins and peptides were searched against the same custom databank as for the secretome samples, in order to identify the VHH. Carbamidomethylation was set as a static modification, and Methionine Oxydation was set as a variable modification. Moreover, due to the deglycosylation, asparagine to aspartate was set also as a variable modification only for samples subjected to the deglycosylation. Parameters were set to 1 peptide per protein, 3 miss cleavage, with no limitation for FDR in order to identify all the potential peptides in the sample. Mass tolerance was also 10 ppm for the precursors and 0.6 ppm for the fragments.

Alignments of peptidic sequences

For the alignments of the variable parts of antibodies, and for some of the constant parts of the antibodies, peptides were identified in different entries of the protein databank because of a high variability in the peptidic sequences. To align all the peptides obtained by MS, entries of the same part of the antibodies were aligned first in MultiAlin (http://multalin.toulouse.inra.fr/multalin/), then the consensus was used to perform the alignments. All the peptides identified were highlighted directly on the consensus sequence to compare the identified peptides in all the samples.

Western Blots

To detect the presence of immunoglobins in secretomes of segments R1, L and C1 collected 12h and 24h after SCI, Western blots were performed (n = 2). To determine protein concentration in the samples, Bradford method was used. Twelve percent acrylamide gels were loaded with 2.5 µg of proteins of 12 h and 24h samples. After migration, proteins were transferred to a nitrocellulose membrane. Membranes were saturated in a PBS-Tween 0.1% containing 5% non-fat dry milk buffer for 1 hour and incubated overnight at 4°C with peroxidase-conjugated goat anti-immunoglobulins (0.08 µg/mL). After intensive washes with PBS-Tween 0.1%, chemiluminescence revelation was performed. Membranes were then dehybridized for 30 min with 0.2 M citric acid solution. After intensive washes with PBS-Tween 0.1%, membranes were again saturated and incubated overnight at 4°C with a primary mouse anti-GFAP antibody (1:1000), and finally a peroxidase-conjugated goat anti-mouse secondary antibody (0.03 µg/mL).

To detect the presence of immunoglobulins in secretomes of segments R1, L and C1 from rat treated with RhoA inhibitor, injected at lesion site at time of lesion and collected 12 h after SCI, western blots were performed (n = 2). Secretomes of segments R1, L and C1 from rat not treated with RhoA inhibitor and collected 12 h after SCI served as controls. To determine protein concentration in the samples, Bradford method was used. Twelve percent acrylamide gels were loaded with 2.5 µg of proteins of 12 h samples. After migration, proteins were transferred to a nitrocellulose membrane. Membranes were saturated in a PBS-Tween 0.1% containing 5% non-fat dry milk buffer for 1 hour and incubated overnight at 4°C with

peroxidase-conjugated goat anti-immunoglobulins (0.08 µg/mL). After intensive washes with PBS-Tween 0.1%, chemiluminescence revelation was performed.

To detect FC gamma receptor CD16 in DRG ND7/23 cells, an immunoprecipitation was carried out. Anti-CD16 diluted at 1:100 in PBS-Tween 0.02% were added to Dynabeads Protein G and incubated for 4 hours. Afterwards, the protein extracts (1 mg) from ND7/23 cells treated or not with 200 ng/mL of LPS were added and incubated overnight at 4°C. After intensive washes with PBS-Tween 0.02% Protein G beads were eluted with glycine 50Mm pH 2.8 and Tris buffer pH 7.4 was added to neutralize the pH. Protein eluted were separated by SDS-PAGE and transferred onto nitrocellulose membranes. After saturation for 1h with the blocking buffer (PBS-Tween 0.1% containing 5% BSA), the membranes were incubated overnight at 4°C with mouse anti-CD16 (1:500) diluted in blocking buffer. After intensive washes with PBS-Tween 0.1%, membranes were incubated with peroxidase-conjugated goat anti-mouse (0.03 µg/mL). After intensive washes with PBS-Tween 0.1%, chemiluminescence revelation was performed.

To detect FC gamma receptor CD32 in ND7/23 DRG cells, 40 µg of total cell extracts were analyzed by Western blotting. Proteins were separated by SDS-PAGE and transferred onto nitrocellulose membranes. After saturation for 1h with the blocking buffer (PBS-Tween 0.1% containing 5% BSA), the membranes were incubated overnight at 4°C with rabbit anti-CD32 (1:500) diluted in blocking buffer. After intensive washes with PBS-Tween 0.1%, membranes were incubated with peroxidase-conjugated goat anti-rabbit (0.08 µg/mL). After intensive washes with PBS-Tween 0.1%, chemiluminescence revelation was performed.

Spinal cords sections and Immunofluorescence

Spinal cords, after being collected, were fixed in 4% paraformaldehyde. They were then submerged in sucrose baths of increasing concentration of 10 to 30% over 3 days before being included in 2% cellulose and frozen at -80°C. and then cut with a cryostat in 20 µm thick sections. For IHC, sections were dried in desiccator for 5 minutes, followed by antigen retrieval in tris-HCl 20mM pH 9 by 30 seconds microwaves treatment. Sections were then rehydrated by 3 baths of phosphate buffer (PBS 1X), before saturation in PBS 1X containing 1% BSA buffer, 1% ovalbumin, 0.05% triton and 1% normal donkey serum. Alexa Fluor® 647-conjugated goat anti-rat IgG (4µg/mL) and mouse anti-NeuN (1:500) were then deposited for incubation overnight at 4°C. Sections were then washed 3 times with PBS, before incubation for 1 hour at 37°C with Alexa Fluor® 488-conjugated donkey anti-mouse IgG (2µg/mL).

CD16 and CD32b immunostaining and fluorescence quantification.

In pursuance of detecting the targeted Fc gamma receptors, 35,000 ND7/23 cells were grown on cover slips and treated or not beforehand with LPS (200ng/ml) and RhoA inhibitor (1µg/mL) for 24 hours. The cells were fixed with paraformaldehyde 4% (PAF) for 10 min, washed in PBS1X (phosphate buffered sodium 1X), and quenched with glycine 50mM. After, cell membrane permeabilization with 0.2% Triton X-100 for 10 min, cells were immersed in a blocking buffer (PBS 1x containing 1% bovine serum albumin,

1% ovalbumin, 1% NDS) for 1 hour. The cells were then incubated overnight at 4°c with rabbit anti-CD32 (1:100) or mouse anti-CD16 (1:100) diluted in the blocking buffer. Washes with PBS 1x were performed and followed by 1h incubation at 37°C with Alexa Fluor® 488-conjugated donkey anti-rabbit or Alexa Fluor® 488-conjugated donkey anti-mouse diluted at 2µg/mL in the blocking buffer. The cells were further washed with PBS 1X and nuclei were stained with Hoechst 33,342 (1:10 000). After a final wash in PBS 1X, cover-slips were mounted using Dako fluorescent mounting medium. Fluorescent stained cells were analyzed using a confocal microscope (Zeiss LSM700) and the quantification was performed by ImageJ software. To that end, 10 fields representative of the well were selected from each condition and circularity, area, mean fluorescence as well as the background of each cell presented in the field were measured. Fluorescence intensity was calculated with the total corrected cellular fluorescence (TCCF) equation = integrated density – (area of selected cell × mean fluorescence of background readings). The results are presented as means ± SD. The statistical significance was evaluated through student's t-test and values of $p < 0.05$ were considered statistically significant (*p-value of < 0.05).

Investigation of the Fc gamma receptors biological effects in ND7/23 DRG cells

To study the role of the CD16 and CD32 receptors ND7/23 DRG cells were placed in serum-free medium containing 1% L-glutamate, 100 U/ml penicillin and 100 µg/ml streptomycin. Afterwards, cells were treated during 1h with 1µg/mL of RhoA inhibitor and then incubated for 24h with rabbit anti-CD32 (1:600), mouse anti-CD16 (1:100) and mouse anti-GFAP (1:500) Mouse anti-GFAP displayed an IgG2 isotype and served as a control of Fc gamma receptors activation. Following these treatments, neurites length has been measured through Image J software and the statistical significance was evaluated by One-Way ANOVA followed by Tukey-Kramer Test (GraphPadInStat 3.0).

Calcium Homeostasis analysis in ND7/23 DRG cells

They were then treated with rabbit anti-CD32 (1:500) and mouse anti-CD16 (1:500) for 24 h and loaded with 2.5 µM Fura-2 AM. After intensive washes with culture medium, fluorescence intensity of Fura-2 in cells was recorded at 340 and 380 nm using MetaFluor Software. The ratio F340/F380 was calculated to evaluate the variations in cytosolic Ca^{2+} concentrations. After 100 seconds of monitoring, 1 µM of thapsigargin was added to induce Ca^{2+} efflux from the ER. This led to the activation of store-operated channels (SOCs) located at the plasma membrane increasing Ca^{2+} intake into the cells.

Transcriptomic studies

To study *Fcgr3* (*CD16)* expression in ND7/23 DRG, RNA were extracted from ND7/23 cells stimulated with 200 ng/mL of LPS using Tri Reagent according to the manufacturer's instructions. 2µg of RNA were treated with 2 units of DNase RQ1 and retro-transcribed using the SuperScript® III kit. To perform RT-PCR experiments, the following primers were used: Rat *Fcgr3* (forward primer: 5'- CAC AGT CAA TGA CAG TGG – 3'; reverse primer: 5'- TTG GAC ACA TGC ATT GTC – 3'). cDNA amplification was performed using

GoTaq polymerase and 40 cycles at 95°C/30 s, 60°C/1 min and 72°C/1 min. Amplicons were then purified, subcloned into pGEM-T easy vector and sequenced.

To study Rat *IgG2c* gene expression in N27 and ND7/23 cell lines, RNA were extracted from ND7/23 or N27 cells were extracted using Tri Reagent according to the manufacturer's instructions. 2µg of RNA were treated with 2 units of DNase RQ1 and retro-transcribed using the SuperScript® III kit. To perform RT-PCR experiments, the following primers were used : Rat *IgG2C* (forward primer: 5'- TCC GTG AAG CTC TCT TGT GC-3'; reverse primer: 5'- ATG GAG GCC TGG GAG GGA CGG – 3').

To study *Rag1* and *Rag2* gene expression in DRG cells (ND7/23), and N27 neurons were stimulated 24 hours with 10^{-4}M of H2O2. DRG cells were also stimulated by secretome from 1 day lesion segment of SCI. RNA were extracted using Tri Reagent according to the manufacturer's instructions. 2µg of RNA were treated with 2 units of DNase RQ1 and retro-transcribed using the SuperScript® III kit. To perform RT-PCR experiments, the following primers were used: Rat *Rag1* (forward primer: 5'- GGC CAT CCG TGT CAA TAC CT-3'; reverse primer: 5'- ACC GAA CTG CCT TTT CTG GA-3'), *Rag2* (forward primer: 5'- GCC TTC TAC CCA AAG AAC CAC-3'; reverse primer: 5'- ACA GTC CCG TTT CCC ATG TT-3'), *Actin* served as referent gene forward primer: 5'- TTG TAA CCA ACT GGG ACG ATA TGG-3'; reverse primer: 5'- GAT CTT GAT CTT CAT GGT GCT AGG-3').

RNASeq data reuse analyses

RNAseq libraries were obtained from the Sequence Read Archive (SRA) database. SRX11310972 corresponds to the dorsal root ganglion (DRG) explant. By contrast SRX7119488 and SRX10720738 are issued from primary neurons from DRG. Blast search was carried out on each databank to reach CD markers and immunoglobulin heavy & light chains. Initially, the search was carried out with a maximum of 100 reads then for the expressed proteins, a second analysis was carried out with 500 reads. The alignment has allowed to identify reads at the 5' end. Those reads recovered the complete constant chain as well as the V(D)J region, which were confirmed using the IgBlast tool. The reads identified with a variable part were aligned with the constant part of kappa light chain.

Results

In a past study proteins involved in the Memo-RhoA-Diaph1 and Rho-Rock pathways were demonstrated in both lesion and caudal 1 segment on day 3 to 10 post-SCI. On the opposite, rostral 1 segment was characterized by a pro-regenerative inflammatory profile favoring the attraction of neutrophils and T regulatory cells as well as a polarization of macrophages/microglia toward a repair promoting M2 phenotype [12]. Accordingly, in these segments, many proteins promoting neurogenesis (neurotrimin, neurofascin, semaphorins) and synaptogenesis (septins, syntaxins, synapsins) were characterized. Such proteomic profiles contribute to settle on both parts of the lesion a pro-neurite outgrowth medium [12]. Unfortunately, these phenomena are not only asynchronous but hampered by the development of a repair-inhibiting process that takes place within the lesion itself and the adjacent caudal segment

(thereafter referred to as C1 segment). In these segments, activation of the Rho-Rock pathway, pro-inflammatory signals, glial scar-promoting molecules prevent the neurite outgrowth process initiated both in the adjacent rostral segment and the distal caudal one. Our objective was therefore to provide a precise description of time- and segment-specific inflammatory events and to identify new immune-related therapeutic targets in SCI. As a proof of principle that our model is well suited to assess the impact of inflammation of SCI, we first performed *in vivo* experiments using the anti-inflammatory agent, FK506 [12]. Results showed that FK506 slightly improved synaptogenesis and neuritogenesis as revealed by anti-synaphysin I and anti-GAP43 labelling and increased the BBB score from 2 to 8 ± 2 in 2 weeks compared to untreated SCI rats. These results reflect that inflammation modulation can improve BBB score and synaptogenesis but not neurites outgrowth [12]. Therefore, it is not sufficient to greatly improve the regeneration process. In these conditions, we decided to deeply analyze the events occurring at early stages of the lesion *i.e.* 12h and 24h after SCI.

Spatio-temporal organization of inflammatory response and neurogenesis at acute stage

We studied protein content of secretomes collected from Rostral 1 and 2 (R1, R2), lesion (L) and caudal 1 and 2 (C1, C2) spinal cord slices extracted 12h or 24h after SCI. After in solution digestion of secretome proteins, we proceeded to a nanoLC-HRMS in MS/MS mode analysis (**Supp. Data 1, Figure 1 inset Table 1**). Collected data were analyzed, multi-samples tests were performed, and a hierarchical clustering was obtained (**Figure 1**). Two main branches were detected. The first isolated lesion secretomes (12h and 24h) from secretomes of other segments. In lesion secretomes (Cluster 1), the more abundant proteins were inflammatory proteins (CRP, CXCL1, 2,3, interleukin 6), complement proteins (Cfi, C5, C1qc, C1r, C1s, C1qbp, C1q, C2, C3, C4, Cfp, C8g, C8a, C9, C6, Cs), calreticulin, metalloproteinase inhibitors 1 and 2, cathepsins B and D (**Figure 1 inset Table 1**). Noteworthy, secretomes from C1 at 24h clusterized with the secretomes of lesion segments, which confirm and extend our previous data showing that, at later time points, lesion and C1 caudal segments harbored similar proteomic profiles (Cluster 2) (**Figure 1 inset Table 1**). Overexpression of complement components, characteristics of innate immune response, was initially restricted to the lesion segment before spreading essentially in C1 segment between 12h and 24h *i.e* during the acute phase of SCI-associated inflammation. Secretomes from other segments partially clusterized depending on the time course and location. Thus, secretomes from rostral and caudal segments collected 12h after SCI were enriched in neurogenesis inhibitors such as Nogo and Neuroendocrine-Specific Protein (NSP) (Cluster 3) (**Figure 1 inset Table 1**). On the opposite, after 24h, proteins promoting neurogenesis (Robo 1 and 2, Plexin B1, Semaphorins 6d and 4b, Neuronal Cell adhesion molecule 1 and 2 (Ncam1 and Ncam2) were highly represented in secretomes from caudal and rostral segment (**Figure 1 inset Table 1**). It is especially interesting to notice that the inflammatory response intensity raised between 12h and 24h, and that proteomic profiles of rostral and caudal segments changed in this time window. Proteomic study of the acute phase, at 12h and 24h, also demonstrated the presence of immunoglobulins. Immunoglobulins found were IgG (IgG1, IgG2a, IgG2b,

IgG2c) (**Tables 2 and 3**). Of note, IgGs were abundantly detected in spinal cord slices at early time points following SCI. We previously showed the presence of IgGs in the supernatants of SC slices at 3 days (3D), 7 days (7D) and 10 days (10D) after SCI [4]. Since B-cells were not detected in the spinal cord parenchyma during SCI we concluded that, yet unknown mechanisms supported the capture and subsequent release of IgGs from spinal cord slices [4]. Their presence at such early time (12h) is surprising, and knowing that IgGs, depending on their subtype, have different receptors and functions, such as the ability to fix complement, it has been decided to focus on these immunoglobulins for further work. We thus performed an in-depth analysis to further decipher the time-course of IgGs release from SC slices in SCI.

Meta-analysis of the SCI data

Except in shark and camel, where minibodies have been identified as dimer of shortened heavy chain of immunoglobulins [13, 14, 15, 16], for most vertebrate species, antibodies are composed of four polypeptidic chains, two heavy chains and two light chains, linked by disulfure bounds [17]. Heavy chains are subdivided in four domains, Variable Heavy (VH) , Constant Heavy chains (CH1, CH2 and CH3), whereas light chains are subdivided in two domains, Variable (VL) and Constant (CL) [17]. In the variable domains (VH and VL), hypervariable regions (CDR for complementary determining regions) and variable regions (FR for framework) are present, determining the paratope of the antibody. Meta-analysis performed from shot gun proteomic based on spatio-temporal study of spinal cord injury from 12h to 10 days, performed on triplicate data, gave evidences of IgGs isotypes with a sequence coverage of 48,52% [4, 5, 12]. The most abondant were IgGs, especially IgG2a and IgG2B, but constant kappa light chain was also found with high LFQ values (**Table 2**). Indeed these immunoglobulins as well as Lambda constant chain were detected in the secretome all along the spinal cord whatever the time after lesion and the segment. Of note, some immunoglobulins (IgG1, IgG2a, IgG2b, constant kappa and lambda light chains) were also identified in the segments from the control group (**Table 2**). For IgG2a, the most part of the identified peptides whatever the conditions covered the CH2 and CH3, one single peptide was detected in CH1 (**Supp. Data 2**). For IgG2B, CH2 was mostly covered and one peptide in CH3 was found whatever the time and the spatial localization (**Supp. Data 2**). Concerning lambda chain, almost 93% of the constant part has been identified (**Table 2 + Supp. Data 1).** It is interesting to note that IgM and IgG2c were also identified but almost exclusively 12h after the lesion. It means that release of these immunoglobulins was induced by the lesion and not present natively in the spinal cord **Table 2**, **Supp Data 2**). Indeed, IgG2c and IgM-like protein were detected mostly in secretomes from Lesion and Rostral segments at 12h and then in Lesion and Caudal segments at 1D. This fits with the slide from rostral to caudal segments previously demonstrated in whole proteomic studies [4]. This time windows is clearly unusual for IgM production which appears normally 6 to 7 days after trauma. We also observed that IgG2c diseapered afterwards and IgM slightly decreased from 3D and its production stayed centered at the lesion site. For IgM, differents peptides covering parts of the heavy chain were identified (**Supp. Data 2**). At this time window (12H, 24h), we also identified of a heavy variable part with a coverage of 54% (**Table 2, Supp. Data 1**). At the lesion site 12h after SCI, variable parts of Kappa and Lambda light chains were also

detected. Lambda V then disappeared whereas Kappa V spread in all segments at 24h and then disappeared. Only 40% for the VL were identified whereas almost 80% for the VK were characterized (**Table 2, Supp Data 2**). To assess more accurately the spatio-temporal evolution of immunoglobulin levels in the secretomes after SCI, their LFQ values were normalized to those quantified in the secretomes of controls (non-lesioned spinal cord) (**Figure 2A**). This confirmed that IgG1, IgG2a, IgG2b and IgG2c appeared increased between 5 to 15 times from 12h to 24h in rostral 1, lesion and caudal 1 segments. Moreover, at 24h, the levels of IgGs increased only in caudal 2 segments. These levels began to decrease from 3 days and became low at 7 days. Moreover, this analysis revealed again that immunoglobulins showed a trend to be higher at the lesion site. To complete our study, Western blot anti-IgG analyses were carried out on secretomes of lesion, rostral 1 and caudal 1 segments harvested 12h and 24h after SCI. These experiments were conducted in denaturing and reducing conditions (**Figures 2A**). Two biological duplicates were loaded on each gel. These experiments confirmed the presence of heavy and light chains detected at 50 KDa and 25 KDa respectively. In gel digestion was also performed in parallel and validated the identity of these bands as heavy and light chains (**Supp. Data 3**). Previously, during our proteomic analysis, we detected constant levels of GFAP in these secretomes[12]. Therefore, we decided to use this protein as an internal control during our western blot experiments. The intensity of heavy and light chain bands was quantified and normalized to those of GFAP. Even if no significant differences were found, heavy and light chains again showed a trend to be higher at the lesion site, especially at 24h after SCI (**Figure 2B**).

Immunoglobulins are detected in the normal CNS

As described above, we identified immunoglobulins within the control spinal cords, the question arose of the origins of such released immunoglobulins in the spinal cord under steady state conditions. The release of immunoglobulins from SC slices could be a consequence of the experimental setting during which tissue slicing and subsequent short-term organotypic cultures are likely to alter the physiological behavior of neural cells. To address this issue, we extracted proteins from a freshly frozen intact spinal cord, avoiding thus any culture bias, and found similar results (**Figure 2C, inset Table 4**). Since neural cells express receptors of the constant fraction (Fc) of immunoglobulins [18], one may propose that the presence of IgGs from spinal cord neural cells is primarily conditioned by their transport from blood to brain and their subsequent internalization and release by neural cells. However, intriguingly, a survey of the mouse Brain atlas showed that mRNA expression of IgG1 and IgG2 classes in distinct CNS regions including the spinal cord, cerebellum and hippocampus in both juvenile and adult mice (http://mouse.brainmap.org/) (**Supp. Figure 1A**). Altogether these results, support that immunoglobulins are present in basal state in spinal cord.

Tissues SCI immunogobulin identification

Antibodies are mostly identified from biological fluids and mass spectrometry has highly contibuted in that direction using shot gun proteomic [19] or top-down proteomic [20, 21]. By contrast, immunoglobulins present in complex samples such as tissues are more difficult to characterize. In order to isolate and further characterize IgGs in tissues, enrichment of IgGs may be necessary. Conventional enrichment of IgGs in complex samples are based on affinity chromatography with protein A, protein G or antigen, and can be followed by mass spectrometry analysis [22]. However, a novel and alternative technique named the Melon gel is also possible but is mostly used to purify IgGs from serum. More precisely, the Melon gel is not an enrichment technique but is based on negative selection thanks to a resin which capture all the proteins except the IgGs. To the best of our knowledge, this technique is used exclusively on serums and not on protein tissue extracts [23, 24, 25], so it was decided to test Melon gel on protein extracts from tissue as well. Enrichment procedure using ammonium sulfate precipitation, Melon gel purification was performed on spleen as a contol and spinal cord lesion segment withdrawn seven days after injury (SCI 7D-L) (**Figure 3 inset Table 5, Supp Data 3**). After the MS analysis with MaxQuant, IgG were detected, confirming the efficiency of the tissues extract and immunoglobulin enrichment procedure. Light chains Lambda C, Kappa C, Kappa V were detected in both spleen and SCI extracts 7 days after lesion as we previously found in secretome. Only IgG2A, IgG2B are detected in SCI extracts 7 days after lesion whereas no IgM or IgG2C were detected at 7 days (**Figure 3 inset Table 5**). To extend our study, we validated the presence of immunoglobilins in SCI tissue by immunofluorescence (**Figure 3**). Co-labeling was performed with anti-NeuN (neuronal marker) and anti-IgG on sections of lesion segments from spinal cord collected 24 hours after lesion (**Figures 3(A-C)**). This revealed that cells around the lesion site stained with anti-IgG were neurons since they were also labelled with anti-NeuN. We previously demonstrated the impact of RhoA pharmacological inhibition on neurites outgrowth and synaptogenesis [12]. This was confirmed by shotgun proteomics performed on rostral, caudal and lesion segments collected 12h after lesion with or without treatment with RhoA inhibitor (**Supp. Figure 3**). This revealed that inflammatory proteins and immunoglobulins were more abundantly present in lesion site with or without RhoAi treatment (Cluster 1). By contrast, Cluster 2 showed proteins involved in synaptogenesis which, were more highly detected after RhoAi treatment. Cluster 3 represented proteins involved in neurite outgrowth such as CNTF, contactin, Neural Cell Adhesion Molecule L1, Stathmin, Neurofascin, Neurotrimin and Dynactin. These proteins were more abundantly detected in R1 and C1 segments without RhoAi treatment. We thus evaluated at early stage after SCI, the impact of such a RhoA inhibition (RhoAi) on IgG levels released by spinal cord explants (**Supp. Data 5**).

RhoA inhibition increased IgG release by spinal cord explants

RhoA inhibitor was injected at lesion site at time of lesion and SCI explants were collected at early stage after SCI *i.e.*, 12H. A shot gun proteomic analysis was then conducted on secretomes from the various segments (**Figure 4Aa**). The LFQ values obtained for IgG were compared to those measured in

secretomes of SCI explants from rats untreated with RhoA inhibitor. This revealed that RhoAi treatment increased the release of the various IgG isotypes considered in this study. In section R2, C1, C2, fold changes reached 3 to 4, whereas in R1 and lesion fragment, fold change reached 2 to 3. Western blot analysis in reducing conditions confirmed again the presence of IgG in these secretomes (**Figure 4B**). Afterwards, semi-quantitative analysis of IgGs in spinal cord tissue sections confirmed the impact of RhoAi treatment in the R1, C1 and lesion segments (**Figure 4Ab**). Interestingly, while IgG1 and IgG2C were the most prevalent isotypes in the spinal cord secretomes of non-treated injured animals, IgG2A was the most abundant IgG isotype in the spinal cord secretome of RhoAi-treated injured animals, especially at the lesion site (**Figure 4A**). Besides IgG2A, we also observed an isotype-specific effect of RhoAi treatment for other IgGs. After treatment with RhoA inhibitor, IgG2C along with IgG1 highly increased in the secretome of the lesion segment while conversely IgG2C was not detected in R1, decreased in Lesion and was predominant in C1. IgG2A greatly increased in lesion (**Figure 4A**). These results indicate that RhoAi treatment induced an isotypic commutations (systemic or local) and/or an isotype-specific mechanism of capture and release of IgGs by neuronal cells.

Neurones produce IgG

To determine if these IgG were synthesized or recaptured by neurons, a transcriptomic approach was undertaken in Dorsal root ganglia (DRG) ND7/23 cell line stimulated with LPS to mimic an inflammatory condition as observed at the lesion site. Moreover, the same approach was performed in the non-differentiated N27 neurons (N27). Transcripts from spleen serve as a positive control. By RT-PCR, we amplified the whole IgG2c ORF in N27 neurons as another source of neurons. Cloning was performed and sequencing confirmed that this gene was expressed in N27 cells demonstrating the neuronal origin of these immunoglobulins (**Figure 5A**). These results are in line with recent data showing the expression of the genes encoding IgG3 and IgM in murine spinal and supraspinal neurons [26]. Allen Brain Atlas confirms in mouse the presence of IgG3 and IgH-VS107 immunoglobulins chains in cortex and hippocampus regions (**Supp. Figures 1A and 1B**) **or** spinal cord (**Supp. Figure 2**)**.** Analyses of RNAseq Data provided Sequence Read Archive from rat DRG neurons confirmed the expression of immunoglobulins heavy and light chains (constant and variable) (**Figure 5B**, **Supp. Table 1, Supp. Data 4**). We identified constant heavy chain of IgG1, IgG2(a, b), IgM, Kappa and Lambda in DRG explant and IgG2(a, b), IgM, Kappa heavy chains in primary culture of DRG neurons. Several V(D)J chains were also identified associated with the Heavy constant chain of IgG2(a,b) and Kappa chains (**Figure 5B**).Taken together, presence of immunoglobulins in neurons is comforted. Moreover, it is well known that Immunoglobulin superfamily proteins (IgSF) are implicated in diverse steps of brain development, including neuronal migration, axon pathfinding, target recognition and synapse formation as well as in the maintenance and function of neuronal networks in the adult [27]. To support Ig production by neurons, we studied in DRG and N27 cells, expression of genes encoding the enzymes Rag1 and Rag2 controlling V(D)J recombination. Since during SCI or other brain trauma, an important amount of neuronal death is observed, we thus mimic this process by using H2O2 treatment [28]. Under that condition, *Rag1* expression was only observed in N27

cells whereas *Rag2* mRNA was detected in both cell lines. (**Figure 5C**). Since *Rag1* expression may be induced by specific factors produced after SCI, DRG cells were cultivated in the presence of secretome of lesion segment collected one day after lesion representing the acute phase of inflammation after SCI (**Figure 5C**) [12]. In such condition, *Rag1* expression was observed. These results suggest that neurons produce a variability of immunoglobulins through V(D)J recombination.

Identification of FcγRs (CD16, CD32) in DRG ND27/3 neurons

In the immune system, immune response modulation by IgGs involves the Antibody-Dependent Cell-Mediated Cytotoxicity (ADCC) mechanism [29]. In this context, IgGs through their paratopes recognize their target and label the cells to be destroyed. For this purpose, cytotoxic immune cells recognize the bound IgGs through their constant region. This recognition involves FcgR such as CD64, CD32 and CD16 expressed at the cell surface of cytotoxic cells. For a long time, it was considered that the expression of these receptors was restricted to immune cells. However, recent studies have demonstrated the presence of FcgR I (CD64) at the cell surface of glial cells such as microglia and astrocytes [30]. More recently Zhang and collaborators also established that FcγRI, but not FcγRII (CD32) and FcγRIII (CD16), was also expressed in a subpopulation of primary sensory neurons [31]. Allen Brain Atlas indicated that Igs are colocalized with CD16 and CD32b in the same mouse brain region (**Supp. Figures 1C and 1D**). At a first step, to demonstrate the expression of CD16 and CD32 receptor, we used a transcriptomic and Western-Blot approaches in DRG ND27/3 cells (**Figure 6**). RT-PCR experiment was carried out to amplify *Cd16* transcripts. A positive fragment was obtained, and sequencing confirmed the expression of this gene in DRG ND7/23 cells (**Figures 5A & 6B**). These results are in line with rat RNAseq DRG analyzes (**Figure 5 inset Table 6**). To confirm the expression of CD16 at the protein level, Western blot experiment was conducted after immunoprecipitation with an anti-CD16 performed on protein extracts from DRG ND7/23 cells stimulated or not with LPS (**Figure 6C**). LPS stimulation was used to mimic an inflammatory condition as observed during SCI. In both conditions, a band close to 30 KDa and corresponding to CD16 was revealed. An additional band close to 52 KDa was also observed. It has been described that efficient cell expression of CD16 requires its interaction with a dimer of Fcer1g [29]. Fcer1g mass is close to 10 KDa. Therefore, the band around 52 KDa observed in our experiment may correspond to CD16 bound to Fcer1g dimer. Altogether, this confirmed the expression of CD16 in DRG ND7/23 cells. Interestingly, under LPS treatment the intensity of the bands increased compared to the control condition. This pinpointed that inflammatory environment mimicked by LPS regulated CD16 expression in sensory neurons (**Figures 6C**). To test the activation of CD16 through anti-CD16 intracellular calcium release[32] was registered (**Figure 6D**), confirming its activation. To identify CD32b receptor in DRG cells, Western Blot analysis was also conducted and revealed a band at 34 KDa matching with its molecular weight (**Figure 7A**). This receptor is known as the only inhibitory receptor of the FcγR family since it's the only one expressing the

ITIM motif on its cytoplasmic domain. These results are in line with RNAseq data (**Figure 5 inset Table 6**). Moreover, we observed that RhoA inhibition increased IgG release by SCI explants (**Figures 7A**). In macrophages, it has been shown that CD32b expression was also increased by LPS treatment [33]. Therefore, to determine if RhoA inhibition treatment combined or not with LPS could modulate the expression of CD16 and CD32 in DRG ND7/23 cells, we study their expression profile by immunofluorescence (**Figures 7B**). Under LPS and/or RhoAi treatments, the intensity of CD16 immunostaining increased remarkably compared to the control condition. In fact, this intensity was 4%, 40% and 63% higher for LPS, RhoAi and the combined LPS+ RhoAi treatments respectively. In comparison to the control condition, the intensity of CD32 staining was also enhanced by 52%, 72% and 88% for LPS, RhoAi and LPS+ RhoAi treatments respectively (**Figure 7B**). These results suggested the potential involvement of those factors in the upregulation of CD16 and CD32 expression. Moreover, even if anti-CD16 and anti-CD32 were employed at the same concentration, the detection threshold for anti-CD32 was lower. Indeed, in comparison with anti-CD32, the intensity of fluorescence measured with anti-CD16 was 67%, 33%, 30% and 38% more intense for the control, LPS, RhoAi and LPS+ RhoAi treatments respectively (**Figure 7B**). This showed that the expression of CD16 was higher than CD32 under both basal and stimulated conditions. Since RhoAi modulated neurites outgrowth, synaptogenesis [12] and increased IgG release in spinal cord (as well as the expression of CD16 and CD32 in sensory neurons (**Figures 7B & 7C**), we investigated the possibility that activation of these Fc receptors present in DRG ND7/23 cells could modulate neurites outgrowth.

Antibody Dependent Neurite Outgrowth Modulation (ADNM) responses

Before to perform biological neurites outgrowth assays, we confirmed in contrary to anti-CD16 (**Figure 6D**), anti-C32 did not stimulate intracellular calcium release (**Figure 7D**). To test the impact of CD16 and CD32b activation with their specific antibodies on neurite outgrowth, DRG sensory neurons were incubated with anti-CD16 and/or anti-CD32 in presence or not of IgG2 isotype (**Figure 7E**). In comparison with the DMEM control condition, percentage of neurite outgrowth was higher after CD16 activation while CD32b activation had no effect. Moreover, activation of both CD16 and CD32b also led to an increase of the percentage of neurite outgrowth. Keeping in mind that CD32b is known as the only inhibitory receptor of the FcγR family, this showed that CD16 activation could prevail and be sufficient to overcome a potential inhibitory effect exerted by CD32b. To test if CD32b could exert such an inhibitory effect on neurite outgrowth, a stronger activation of CD32b was triggered by addition of a treatment with IgG2 isotype (**Figure 7E**) In its presence, we observed that whatever the conditions, the percentage of neurite outgrowth remained close to the one observed in control conditions with DMEM or IgG2 treatment. In comparison with CD16 activation combined or not with CD32b activation, the percentage of neurite outgrowth was significantly reduced when DRG cells were incubated in the presence of IgG2 isotype + anti-CD16 +/- anti-CD32. Therefore, the activation of CD32b by IgG2 isotype prevented CD16 from triggering neurite outgrowth. Altogether, these results suggest that various IgG according to their isotypes

could modulate neurite outgrowth through the activation of CD16 and CD32b. We named this process Antibody Dependent Neurite Outgrowth Modulation (ADNM) (**Figure 8**).

Discussion

Autoimmune diseases affect about 5–7% of the world population and 3% of these autoimmune diseases involve pathogenic CNS-reactive autoantibodies [34]. Neural repertoires, defined as the whole of neural populations and synaptic circuits supporting the cognitive and sensorimotor functional repertoires [35], express brain autoantigens such as myelin and synapse-derived proteins (Glutamate decarboxylase (GAD2), acetylcholine receptor (AchR), and acetylcholine esterase (AchE)) [36]. Interestingly, some brain autoantigens involved in major CNS functions are targeted in non-CNS autoimmune disorders. Such autoantigens, proposed to be named brain super autoantigens [35], notably include HSP60 and TROVE2, two major autoantigens in rheumatoid arthritis and lupus respectively. HSP60 (*hspd1*) plays a major role in the control of synaptic neurotransmitter release and mutations in *hspd1* gene are responsible for autosomal recessive spastic paraplegia disease [37]. Similarly, SNP variants of *trove2* gene (also knowns as RNA binding protein Ro60 autoantigen), have been associated with higher emotional memory capacity in healthy human subjects [36]. It is thus thinkable that pathological autoimmunity in general is preferentially targeted toward brain autoantigens and reflects the distortion and/or the amplification of a physiological process during which autoimmunity supports cognition and CNS homeostasis [35]. Favoring this view, in Multiple Sclerosis (MS) disease, a recent clinical study on 176 patients identified a large panel of autoantibodies recognizing more than 30 neuronal or glial autoantigens [38]. Similarly, a number of neuropsychiatric disorders like autism spectrum disorder are accompanied by the synthesis of CNS-reactive antibodies [39]. Independently from any consideration on their actual role, autoantibodies are thus emerging as a new generation of biomarkers in CNS disorders, ranging from neurotrauma to neuropsychiatric or neurodegenerative diseases [39]. Interestingly, although brain-derived autoantigens might not be immunogenic under physiological conditions, several pathology-associated events might drive CNS-targeted autoimmunity. These notably comprise the occurrence of immunogenic post-translational modifications and the co-release by neural cells of brain autoantigens and danger signals. In TBI, autoantibodies are directed against a repertoire of CNS self-antigens (proteins) including GM1 gangliosides, myelin-associated glycoprotein, α-amino-3-hydroxy-5-methyl-4-isoxazolepropionic acid (AMPA) and N-methyl-D-aspartate (NMDA) glutamate receptors, and β-III-tubulin and nuclear antigens [34, 39, 40, 41]. Moreover, immunocytochemistry studies performed with monoclonal antibodies as well as fragment antigen binding (Fabs) at the level of the CNS have shown the presence of immunoglobulin isotypes (IgG1, 2A, 2B, 2C), Kappa and Lambda chains [42, 43]. In normal rat brain, IgG are detected, and this level reached a higher amount after head injury [44]. *In situ* hybridization experiments depicted in mouse Brain Atlas also revealed the presence of such immunoglobulins encoding transcripts (IgG and IgM) in hippocampus, cortex, and spinal cord. Moreover, during spinal cord injury (SCI), traumatic brain injury (TBI) and a multitude of other CNS pathological conditions such as multiple sclerosis (MS), an intrathecal synthesis of IgGs is observed [45]. The origin of such intra-CSF (cerebrospinal fluid) IgGs is still

debated. The two main current hypotheses are that IgGs are produced locally by CNS-invading B-cells or are somehow transported from blood to CNS. In several neuroinflammatory pathological disorders, including notably MS, a hallmark of intrathecal IgGs is to form oligoclonal bands (OCBs), which suggests a rather limited diversity of antibodies and, consequently, a finite number of corresponding targeted antigens. While MS pathology is essentially characterized by the existence of multifocal inflammatory and demyelinating lesions (the MS plaques), OCBs develops in the quasi-absence of B-cells in inflammatory lesions. Indeed, OCBs are considered the products of clonally expanded B cells in the cerebrospinal fluid (CSF), representing the sum of contributions from B cells in the brain. However, large amounts of IgGs can be eluted from MS plaques in which lymphocytes are absent. Interestingly, in a recent study analyzing CSF samples from 115 MS patients, it was calculated that 3.2 billion lymphocytes would be necessary to generate such large amounts of intrathecal IgG levels (30 mg in 500 ml CSF) [46]. CSF-circulating lymphocytes were estimated to account for < 0.1% of the IgG levels in MS brains. Such a finding is thus compatible with the possibility that intrathecal IgGs might not derive from intrathecal B-cells [46]. Supporting this fact, the neuronal distributions of IgG are found in motor neurons in brainstem nuclei including trigeminal motor nucleus, facial nucleus, and hypoglossal nucleus [43] and confirmed recently by transcriptomics analyses in mice spinal neurons [26]as well as our immunoflurorescence experiments[4] on rat spinal cord. The present study is in line with these results. Our proteomic data establish that IgG2A and IgG2B are present in spinal cord in control and the level is similar in time course of SCI whereas the protein related to IgM is only express 12h to 24h after lesion. This time window is not compatible with a B cell production since IgM are produced 7 to 10 days after antigen recognition. Accordingly, we demonstrated the expression of IgG2 isotypes encoding genes through RT-PCR experiments performed on CDNA from rat N27 dopaminergic neuronal cell line and data reuse of RNAseq datasets obtained from rat primary culture of DRG neurons. While a pathogenic role has been generally assigned to CNS autoantibodies, a neuroprotective function of natural IgG autoantibodies has also been suggested. In this line, several studies have shown that binding of such antibodies to the surface of neurons through FCγR enhances remyelination and modulate neuronal apoptosis [47, 48, 49, 50, 51, 52]. Consistently, our results demonstrate that CD16 (FcγRIII) activation also modulate neurites outgrowth. Taken together, all these data show that autoantibodies have two sources of production, peripheric *i.e.* B-cells and central. However, our results suggest that these autoantibodies could not be only involved in immune response as the B-Cells but could also modulate neurites outgrowth. In this context, the cross-talk play between CD16 and CD32b activation in neurite outgrowth process evoked an antibody dependent neurite outgrowth modulation (ADMN). This mechanism could be seen as a counterpart of the Antibody Dependent Cell Cytotoxicity (ADCC) observed during the inflammatory response and involving the same receptors. Indeed, while CD16 activation favors neurite outgrowth, CD32b activation inhibited it. the balance between activation and inhibition could be fine tune by the nature of the various IgGs isotypes released after trauma as we observed during SCI. Moreover, we cannot also exclude that among the immunoglobulin released, some could be involved in inflammation since, the VHH found at 12h present sequence homology with a nanobody directed against RON protein. RON is a Macrophage-stimulating protein receptor and is related to c-MET receptor tyrosine kinase. In brain RON is expressed on

tissue-resident macrophages including microglia [53]. An *in vivo* deletion of the ligand binding domain of Ron (Ron−/−) promotes inflammatory (M1) and limits a reparative (M2) macrophage activation. These results are in line with its expression found at 12h at the lesion site [54]. The possiblitiy that anti-RON could activate microglia 12h after lesion also fits with previous data obtained on microglia activation study [5]. These results can also be correlated with previous studies performed by Popovich group which showed that mice lacking Heavy chain of Immunoglobulins (IgH-6 KO) have an improved locomotor function and reduced spinal pathology compared to wild-type mice after SCI, suggesting a pathogenic role for antibodies [40, 55]. The intraspinal pathology caused by B cells in wild-type mice is due in part to antibody-mediated ligation of Fc receptors and complement activation. But even though intraspinal B cell clusters and autoantibodies are maintained indefinitely in injured mouse spinal cord, there is no proof these immune responses cause protracted neurological deterioration. A precipitous decline in function would be registered in both mice as B cells became activated and autoantibodies were synthesized. B cells and autoantibodies would respond to proteins that are newly expressed in growing axons, remyelinating oligodendrocytes, stem cells or new endothelia. In that case, little or no additional gain of function beyond that achieved prior to the onset of the autoimmune response, would be expected which is not the case. In fact, in animal models of SCI, spontaneous recovery of function is registered after a period of weeks or months post-injury. Taken together, results in wild-type animals tend to show that autoantibodies are not only involved in pro-inflammatory response but also in neuroregeneration. Unfortunately, the IgH-6 KO model fails to confirm this hypothesis because the invalidation blocks the two possible sources of IgG production in the same manner if the IgGs are synthesized by the same mechanism (VDJ recombination). All these evidences support that IgGs and their receptors are involved in neurite outgrowth modulation. This interesting change of paradigm constitutes a ground-breaking advance in the field of both neurosciences and immunology. The story appears even more complex since CNS immunoglobulins seem to have various cellular origins. Indeed, the diversity of immunoglobulins identified during our study *i.e.*, reused of RNAseq datasets obtained from DRG explants and proteomics analysis performed on injured spinal cord, does not fit with the restricted number of IgG isotypes found in DRG sensory neurons. In line with such assumption, our previous immunofluorescence experiment performed on injured spinal cord slices also revealed a staining in astrocytes[4, 12]. A survey of “Geodatasets” (https://www.ncbi.nlm.nih.gov/gds/), the NIH-compiled bank of mRNA expression studies, focused specifically on the mRNA profile of spinal cord astrocytes under inflammatory conditions confirmed that astrocytes were a second source of neural IgGs. Indeed, we found one relevant study in which astrocytes derived from mice suffering from experimental allergic encephalomyelitis were cell-sorted at different time points and assessed about their RNA profiles. Surprisingly, when we reused the supplementary data provided in this work by Itoh and collaborators we found that the mRNA species showing the highest fold changes in EAE spinal astrocytes as compared to control spinal cord astrocytes were indeed mRNAs coding for IgG2c and kappa chains or junction chains [56] (**Supp.** Figure 4). Now the challenge is to clarify the function of these CNS immunoglobulins.

Declarations

Acknowledgements

This research was supported by funding from Ministère de l'Enseignement Supérieur, de la Recherche et de l'Innovation (MESRI), Institut National de la Santé et de la Recherche Médicale (Inserm), I-SITE ULNE (Nobody Project) and Université de Lille. The authors would like to thank Raphaël Decaudin for his contribution to this manuscript.

Author Contributions

Conceptualization, M.S. Methodology, A.C., M.A.K., C.M., O.S., F.V.A, F.R., D.C, I.F. and M.S.; Software M.S.; Validation, M.A.K, D.C. and M.S.; Formal analysis, M.S., , D.C. Investigation, D.C. and M.S.; Resources, D.C., I.F. and M.S.; Data curation, M.S., A.C., M.A.K., O.S.; Writing – Original Draft M.S. Writing - Review and Editing, I.F., F.R., D.D., D.C. and M.S.; Supervision, F.R., D.C. and M.S.; Project Administration, D.C. and M.S.; Funding Acquisition, D.C., I.F., and M.S.

Declaration of Interests

The authors declare no competing interests.

References

1. Wyndaele M, Wyndaele JJ. Incidence, prevalence and epidemiology of spinal cord injury: what learns a worldwide literature survey? *Spinal Cord* **44**, 523-529 (2006).

2. Chen Y, Tang Y, Vogel LC, Devivo MJ. Causes of spinal cord injury. *Top Spinal Cord Inj Rehabil* **19**, 1-8 (2013).

3. Cizkova D*, et al.* Understanding Molecular Pathology along Injured Spinal Cord Axis: Moving Frontiers toward Effective Neuroprotection and Regeneration.

4. Devaux S*, et al.* Proteomic Analysis of the Spatio-temporal Based Molecular Kinetics of Acute Spinal Cord Injury Identifies a Time- and Segment-specific Window for Effective Tissue Repair. *Molecular & cellular proteomics : MCP* **15**, 2641-2670 (2016).

5. Cizkova D*, et al.* Alterations of protein composition along the rostro-caudal axis after spinal cord injury: proteomic, in vitro and in vivo analyses. *Front Cell Neurosci* **8**, 105 (2014).

6. Freund P*, et al.* Nogo-A-specific antibody treatment enhances sprouting and functional recovery after cervical lesion in adult primates. *Nat Med* **12**, 790-792 (2006).

7. Freund P*, et al.* Anti-Nogo-A antibody treatment promotes recovery of manual dexterity after unilateral cervical lesion in adult primates--re-examination and extension of behavioral data. *Eur J Neurosci* **29**, 983-996 (2009).

8. DePaul MA, Lin CY, Silver J, Lee YS. Combinatory repair strategy to promote axon regeneration and functional recovery after chronic spinal cord injury. *Scientific reports* **7**, 9018 (2017).

9. Ulndreaj A, Badner A, Fehlings MG. Promising neuroprotective strategies for traumatic spinal cord injury with a focus on the differential effects among anatomical levels of injury. *F1000Res* **6**, 1907 (2017).

10. Thibault-Halman G*, et al.* Predicting Recruitment Feasibility for Acute Spinal Cord Injury Clinical Trials in Canada Using National Registry Data. *Journal of neurotrauma* **34**, 599-606 (2017).

11. Fehlings MG*, et al.* Riluzole for the treatment of acute traumatic spinal cord injury: rationale for and design of the NACTN Phase I clinical trial. *J Neurosurg Spine* **17**, 151-156 (2012).

12. Devaux S*, et al.* RhoA Inhibitor Treatment At Acute Phase of Spinal Cord Injury May Induce Neurite Outgrowth and Synaptogenesis. *Molecular & cellular proteomics : MCP* **16**, 1394-1415 (2017).

13. Nguyen VK, Su C, Muyldermans S, van der Loo W. Heavy-chain antibodies in Camelidae; a case of evolutionary innovation. *Immunogenetics* **54**, 39-47 (2002).

14. Leslie M. Small but mighty. *Science* **360**, 594-597 (2018).

15. Flajnik MF, Deschacht N, Muyldermans S. A case of convergence: why did a simple alternative to canonical antibodies arise in sharks and camels? *PLoS biology* **9**, e1001120 (2011).

16. Conrath KE, Wernery U, Muyldermans S, Nguyen VK. Emergence and evolution of functional heavy-chain antibodies in Camelidae. *Developmental and comparative immunology* **27**, 87-103 (2003).

17. Murphy K, Weaver C. *Janeway's immunobiology*. Garland Science (2016).

18. Fuller JP, Stavenhagen JB, Teeling JL. New roles for Fc receptors in neurodegeneration-the impact on Immunotherapy for Alzheimer's Disease. *Frontiers in neuroscience* **8**, 235 (2014).

19. Nirmalan NJ, Harnden P, Selby PJ, Banks RE. Development and validation of a novel protein extraction methodology for quantitation of protein expression in formalin-fixed paraffin-embedded tissues using western blotting. *The Journal of pathology* **217**, 497-506 (2009).

20. Nemeth-Cawley JF, Tangarone BS, Rouse JC. "Top Down" characterization is a complementary technique to peptide sequencing for identifying protein species in complex mixtures. *Journal of proteome*

research **2**, 495-505 (2003).

21. Fornelli L*, et al.* Top-down analysis of immunoglobulin G isotypes 1 and 2 with electron transfer dissociation on a high-field Orbitrap mass spectrometer. *Journal of proteomics* **159**, 67-76 (2017).

22. Pradzinska M*, et al.* Isolation and characterization of autoantibodies against human cystatin C. *Amino acids* **48**, 2501-2518 (2016).

23. Konno N*, et al.* Changes in N-glycans of IgG4 and its relationship with the existence of hypocomplementemia and individual organ involvement in patients with IgG4-related disease. *PLoS One* **13**, e0196163 (2018).

24. Mills JR, Barnidge DR, Murray DL. Detecting monoclonal immunoglobulins in human serum using mass spectrometry. *Methods* **81**, 56-65 (2015).

25. Blanc MR*, et al.* A one-step exclusion-binding procedure for the purification of functional heavy-chain and mammalian-type γ-globulins from camelid sera. *Biotechnology and applied biochemistry* **54**, 207-212 (2009).

26. Scheurer L*, et al.* Expression of immunoglobulin constant domain genes in neurons of the mouse central nervous system. *Life science alliance* **4**, (2021).

27. Maness PF, Schachner M. Neural recognition molecules of the immunoglobulin superfamily: signaling transducers of axon guidance and neuronal migration. *Nature neuroscience* **10**, 19-26 (2007).

28. Whittemore E, Loo D, Watt J, Cotmans C. A detailed analysis of hydrogen peroxide-induced cell death in primary neuronal culture. *Neuroscience* **67**, 921-932 (1995).

29. Aicheler RJ, Wang EC, Tomasec P, Wilkinson GW, Stanton RJ. Potential for natural killer cell-mediated antibody-dependent cellular cytotoxicity for control of human cytomegalovirus. *Antibodies* **2**, 617-635 (2013).

30. Ulvestad E*, et al.* Reactive microglia in multiple sclerosis lesions have an increased expression of receptors for the Fc part of IgG. *J Neurol Sci* **121**, 125-131 (1994).

31. Zhang J, Niu N, Li B, McNutt MA. Neuron-derived IgG protects neurons from complement-dependent cytotoxicity. *J Histochem Cytochem* **61**, 869-879 (2013).

32. Lajoie L*, et al.* ADAM17-mediated shedding of FcγRIIIA on human NK cells: identification of the cleavage site and relationship with activation. *The Journal of Immunology* **192**, 741-751 (2014).

33. Nimmerjahn F, Ravetch JV. Fcgamma receptors: old friends and new family members. *Immunity* **24**, 19-28 (2006).

34. Diamond B, Honig G, Mader S, Brimberg L, Volpe B. Brain-reactive antibodies and disease. *Annual review of immunology* **31**, 345-385 (2013).

35. Nataf S. Autoimmunity as a Driving Force of Cognitive Evolution. *Front Neurosci* **11**, 582 (2017).

36. Nataf S. Evolution, immunity and the emergence of brain superautoantigens. *F1000Res* **6**, 171 (2017).

37. Hansen J*, et al.* A novel mutation in the HSPD1 gene in a patient with hereditary spastic paraplegia. *J Neurol* **254**, 897-900 (2007).

38. Prineas JW, Parratt JDE. Multiple sclerosis: Serum anti-CNS autoantibodies. *Mult Scler*, 1352458517706037 (2017).

39. Kobeissy F, Moshourab RA. Autoantibodies in CNS Trauma and Neuropsychiatric Disorders: A New Generation of Biomarkers. In: *Brain Neurotrauma: Molecular, Neuropsychological, and Rehabilitation Aspects* (ed Kobeissy FH) (2015).

40. Ankeny DP, Guan Z, Popovich PG. B cells produce pathogenic antibodies and impair recovery after spinal cord injury in mice. *J Clin Invest* **119**, 2990-2999 (2009).

41. Poletaev A, Boura P. The immune system, natural autoantibodies and general homeostasis in health and disease. *Hippokratia* **15**, 295 (2011).

42. Kozlowski GP, Sterzl I, Nilaver G. Localization patterns for immunoglobulins and albumins in the brain suggest diverse mechanisms for their transport across the blood-brain barrier (BBB). *Progress in brain research* **91**, 149-154 (1992).

43. Aihara N, Tanno H, Hall JJ, Pitts LH, Noble LJ. Immunocytochemical localization of immunoglobulins in the rat brain: relationship to the blood-brain barrier. *The Journal of comparative neurology* **342**, 481-496 (1994).

44. Tanno H, Nockels RP, Pitts LH, Noble LJ. Breakdown of the blood-brain barrier after fluid percussive brain injury in the rat. Part 1: Distribution and time course of protein extravasation. *Journal of neurotrauma* **9**, 21-32 (1992).

45. Kobeissy F, Moshourab RA. Autoantibodies in CNS Trauma and Neuropsychiatric Disorders. (2015).

46. Beseler C, Vollmer T, Graner M, Yu X. The complex relationship between oligoclonal bands, lymphocytes in the cerebrospinal fluid, and immunoglobulin G antibodies in multiple sclerosis: Indication of serum contribution. *PloS one* **12**, e0186842 (2017).

47. Wootla B, Denic A, Watzlawik JO, Warrington AE, Rodriguez M. Antibody-mediated oligodendrocyte remyelination promotes axon health in progressive demyelinating disease. *Molecular neurobiology* **53**, 5217-5228 (2016).

48. Bieber AJ, Warrington A, Pease LR, Rodriguez M. Humoral autoimmunity as a mediator of CNS repair. *Trends in neurosciences* **24**, S39-S44 (2001).

49. Mitsunaga Y*, et al.* Direct evidence that a human antibody derived from patient serum can promote myelin repair in a mouse model of chronic-progressive demyelinating disease. *The FASEB Journal* **16**, 1325-1327 (2002).

50. Vargas ME, Watanabe J, Singh SJ, Robinson WH, Barres BA. Endogenous antibodies promote rapid myelin clearance and effective axon regeneration after nerve injury. *Proceedings of the National Academy of Sciences* **107**, 11993-11998 (2010).

51. Wright BR, Warrington AE, Edberg DE, Rodriguez M. Cellular mechanisms of central nervous system repair by natural autoreactive monoclonal antibodies. *Archives of neurology* **66**, 1456-1459 (2009).

52. Schwartz M. "Tissue-repairing" blood-derived macrophages are essential for healing of the injured spinal cord: from skin-activated macrophages to infiltrating blood-derived cells? *Brain Behav Immun* **24**, 1054-1057 (2010).

53. Dey A*, et al.* neuroprotective role of the ron receptor Tyrosine Kinase Underlying central nervous system inflammation in health and Disease. *Frontiers in immunology* **9**, 513 (2018).

54. Cizkova D*, et al.* Modulation properties of factors released by bone marrow stromal cells on activated microglia: an in vitro study. *Scientific reports* **4**, 7514 (2014).

55. Ankeny DP, Popovich PG. B cells and autoantibodies: complex roles in CNS injury. *Trends Immunol* **31**, 332-338 (2010).

56. Itoh N*, et al.* Cell-specific and region-specific transcriptomics in the multiple sclerosis model: Focus on astrocytes. *Proceedings of the National Academy of Sciences* **115**, E302-E309 (2018).

Tables

Tables 2-3 are in the supplementary files section.

Figures

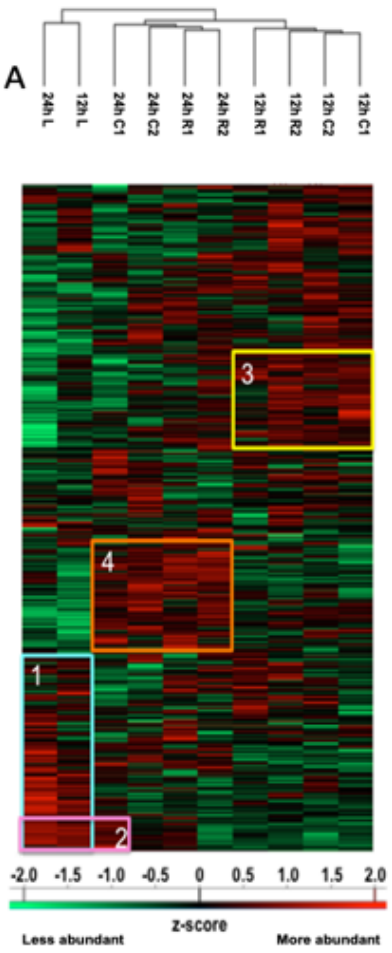

Protein	Uniprot reference	12h R1	12h L	12h C1	24h R1	24h L	24h C1
Immune Response							
C5	A0A096P6L9	27.105	30.753	27.1991	29.8638	31.133	28.256
Complement facteur I	A0A0G2K135	28.6862	31.4865	29.1756	30.9452	31.9867	30.7474
C1q_C	P31722	27.2059	27.5941	27.5216	28.0868	28.9265	27.5725
C8g	D3ZWD6	25.4009	29.3109	25.6515	28.2115	29.3498	27.933
C6	F1M7F7	26.2006	28.4164	25.2068	26.0326	28.8182	26.0147
C9	Q62930	29.3776	32.0729	28.8857	30.5028	32.8296	29.9725
C9	Q62930	29.3776	32.0729	28.8857	30.5028	32.8296	29.9725
Cfb	G3V615	27.5889	29.7907	28.1228	28.8318	30.2445	29.0034
Cfd	P32038	25.8039	29.2837	26.1685	27.3739	29.4617	26.6487
C1s	G3V7L3	25.9108	26.0894	0	0	26.1576	25.6268
C1q B	P31721	26.8409	27.8129	27.6312	27.3534	27.9999	27.1107
C3	M0RBF1	34.5677	35.9915	34.1207	35.4205	36.3782	34.9085
C1q binding protein	O35796	27.1542	28.7074	28.0595	28.183	28.7208	28.348
C4	Q6MG90	28.7578	31.2414	27.9086	29.5244	21.1205	30.2756
Complement C1q A	P31720	26.8299	28.2033	27.1038	28.0575	28.9744	28.2956
C8	D3ZWD6	25.4009	29.3109	25.6515	28.2115	29.3498	27.933
C2	Q6MG73	27.4799	29.0364	0	28.0699	29.841	27.8886
C1q receptor	Q9ET61	0	0	0	0	24.3473	24.4574
CRP	P48199	27.3319	29.1611	26.934	28.2882	29.9143	25.7745
Cathepsin D (ctsd) protease	P24268	29.5102	29.6845	30.016	29.7627	30.1024	29.5429
Cathepsin B (ctsb) protease	P00787	30.6649	31.0627	30.869	31.1476	31.5995	30.7585
Metalloproteinase 1 inhibitor	P30120	31.2912	31.3888	30.293	30.0952	32.0704	30.4234
Metalloproteinase 2 inhibitor	P30121	25.1333	26.2628	26.013	26.0498	26.7354	26.3374
Axonal Guidance							
Roundabout homolog 1 Robo 1	O55005	25.5019	25.6818	25.5182	25.4674	25.7368	26.0018
Protein Robo2	Q9QZI3	26.7878	25.2904	25.377	27.5075	26.8033	28.6504
Neuronal cell adhesion molecule	A0A0G2K329	32.237	32.0057	31.8815	32.527	31.8527	32.2182
Neural cell adhesion molecule 1	P13596	33.6315	33.5348	33.7206	34.7838	34.0443	35.0052
Protein Ncam2	A0A0G2K7P9	29.2571	28.2036	29.191	30.695	29.7085	30.0036
Contactin 4	Q62845	0	0	0	22.7805	0	24.6327
Contactin 6	P97528	0	0	0	24.2783	0	24.4514
Semaphorin 6d	A0A0G2JZC4	0	0	0	24.0672	0	24.8241
Semaphorin 4b	F1LSV0	26.4542	26.0691	26.504	26.7882	25.5816	26.8069
Plexin B1	D3ZDX5	28.3156	28.2094	28.5334	29.5902	27.9306	29.0632

35_37	32_35	29_32	26-29	23-26	20-23	0

Figure 1

Heatmap illustrating hierarchical clustering obtained after analysis of digested peptides isolated in secretomes from spinal cord segments collected 12h and 24h after SCI. 4 clusters are highlighted. Cluster 1 corresponds to the inflammatory proteins accumulation in lesions. Cluster 2 demonstrates that the proteomic profile of C1 starts to cluster with lesions after 24h. Clusters 3 and 4 respectively represent proteins more abundant in other segments at 12h (neurite outgrowth inhibition) and at 24h

(synaptogenesis and neurogenesis proteins). Inset **Table 1.** Label Free Quantification (LFQ) values of proteins found in 12h and 24H secretomes.

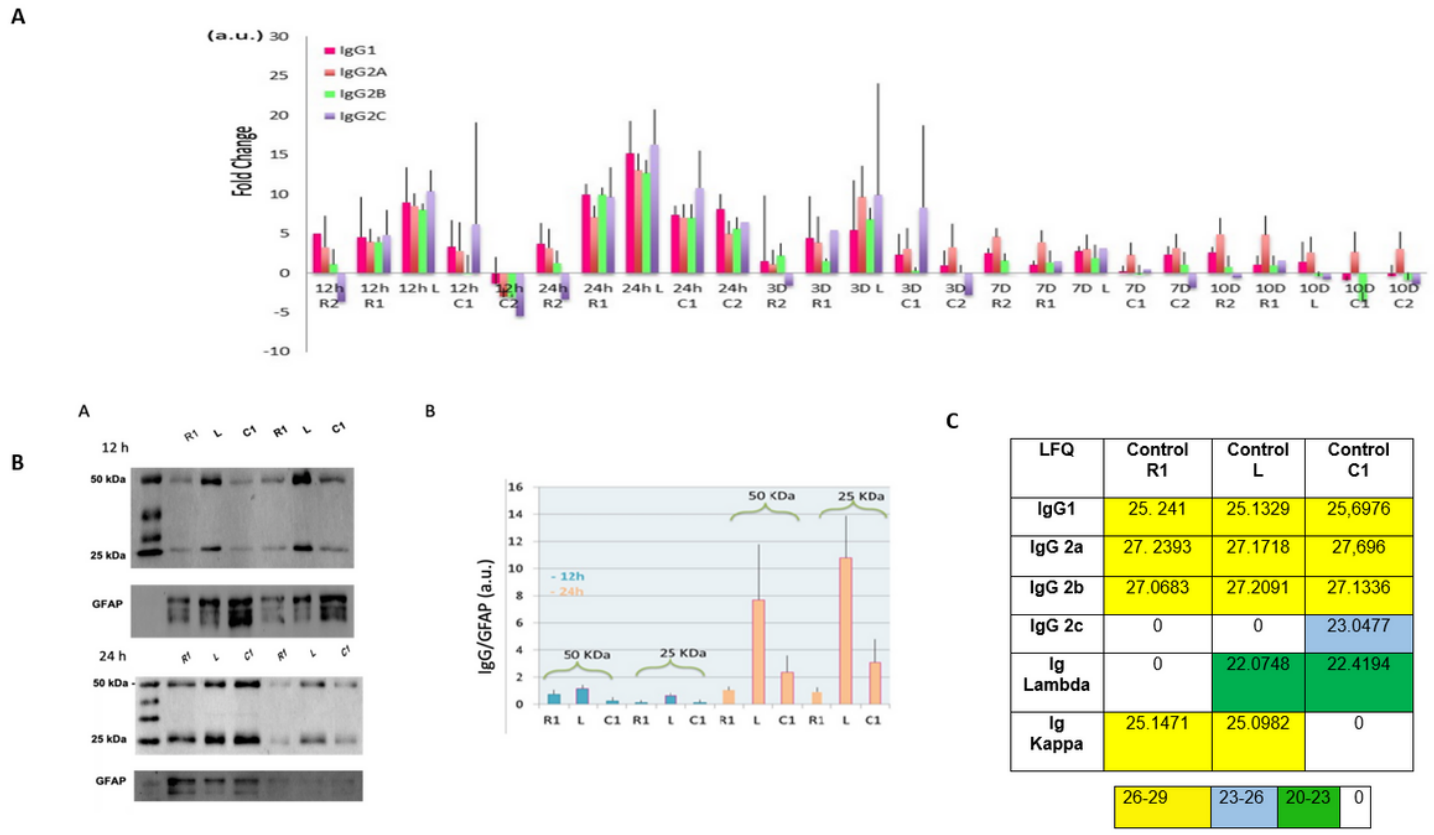

Figure 2

A) Ratio of IgG according to time course after SCI and spinal cord segment. Rationalization was performed by comparing to control (non-lesioned spinal cord) B) : **A)** Western blot of 12 h and 24 h secretomes, with anti-immunoglobulin antibodies **B)** Histogram illustrating the immunoglobulin level as a function of time and segment, obtained by ImageJ software. Results rationalization against GFAP. **C)** Inset **Table 4**: Immunoglobulins rates in control spinal cord. (LFQ : Label Free Quantification).

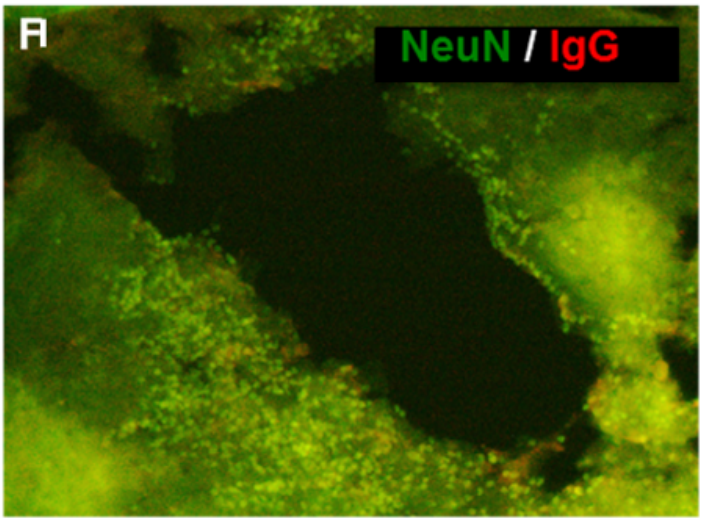

	Tissue	
	Spleen LPS	SCI 7D-L
VHH	NaN	22.9
IgG1	NaN	NaN
IgG2A	31.2	32.5
IgG2B	30.8	30.2
IgG2C	29.1	NaN
IgM	30.7	NaN
Heavy V	NaN	25.1
J chain	NaN	NaN
Kappa C	29.9	30.0
Kappa V	26.4	25.4
Lambda C	28.1	28.6
Lambda V	NaN	24.3

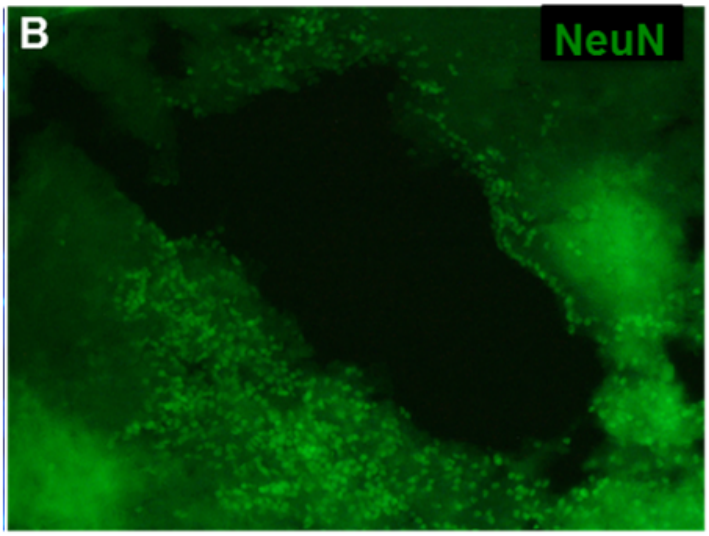

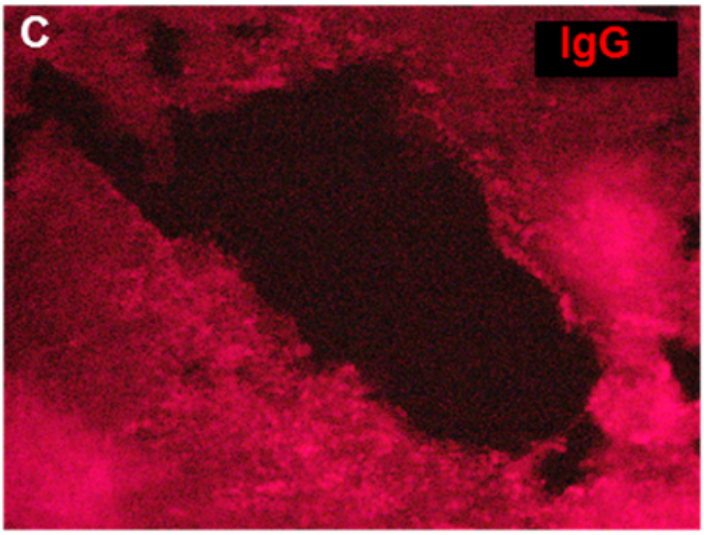

Figure 3

Immunofluorescence performed with anti-NeuN (green, Alexa Fluor® 488) or anti-IgG coupled to Alexa Fluor® 647 (red) from lesion segment section of spinal cord (20X objective). Inset **Table 5**. Sequence coverage in the SCI data from the different isotypes of immunoglobulins from SCI tissues at 7 days after lesion and spleen from rat stimulated with LPS as control.

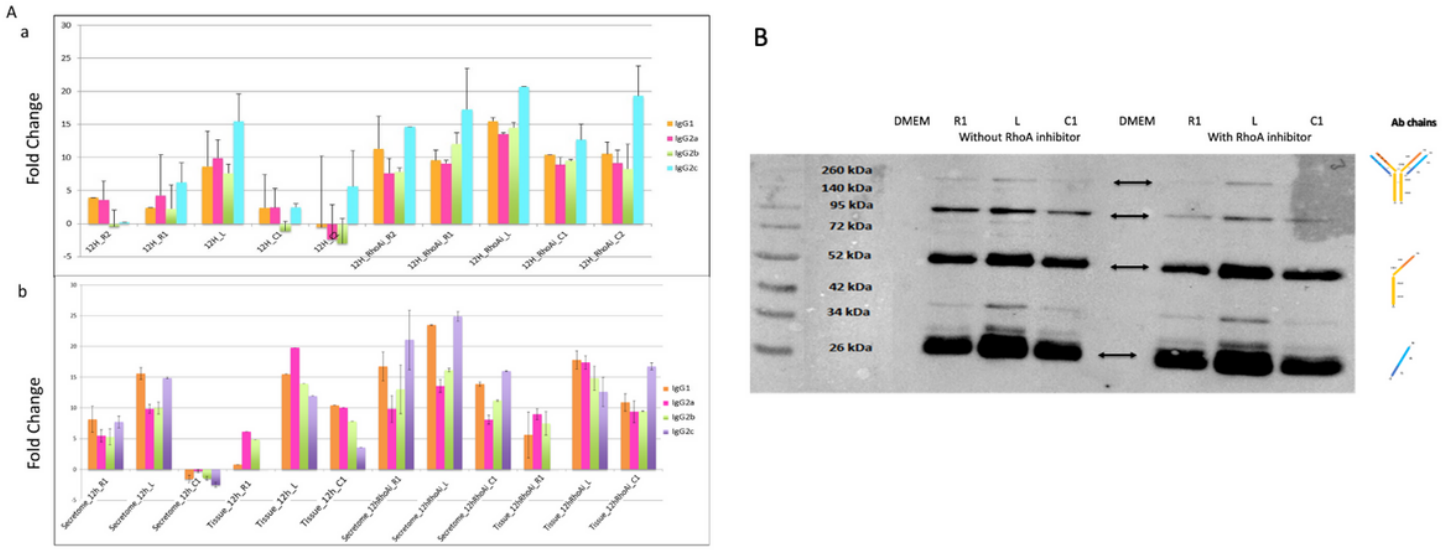

Figure 4

A) a) Fold change between treated and not RhoA inhibitor treatment of IgG isotypes in secretome 12H after SCI in the different segments **b**) Fold change of IgG isotypes between Tissue and secretome **B**) Western blot corresponding of the IgG chains detected in secretomes from rostral, caudal and lesion segments collected 12h after lesion with or without treatment with RhoA inhibitor.

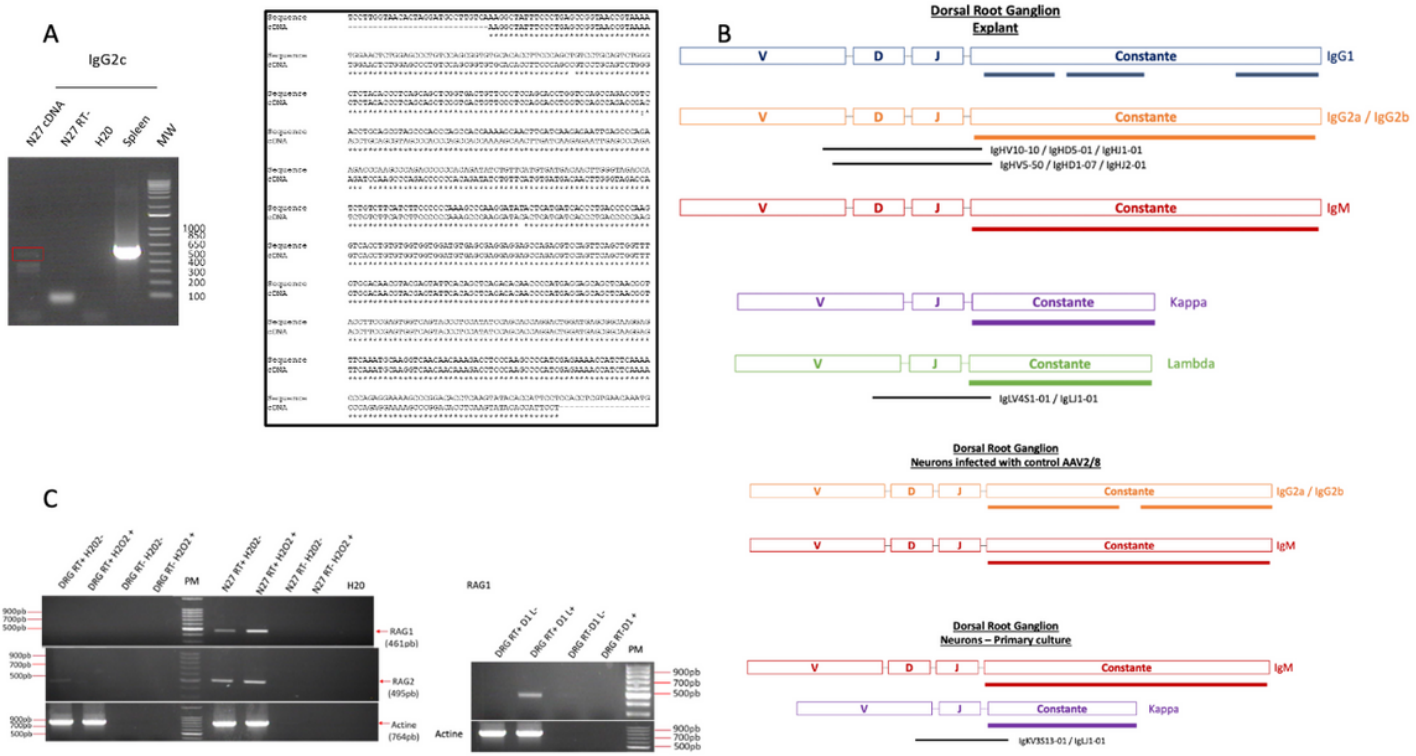

Figure 5

RT-PCR amplification of IgG2c in spleen and in N27 cells, was confirmed by sequencing and inset Table 6 representing RNAseq analyses of DRG neurons for Immunoglobulins transcripts identification. B) Identified immunoglobulins heavy and Light constant chains and variable part from DRG explant or DRG primary neurons according to RNaseq data B (**Supp. Data 4, Supp. Table 1**) C) Amplification of Rag1 and Rag2 mRNA in DRG and N27 cells was carried out by RT-PCR in presence or not of H_2O_2 to induce neuronal death, as observed during the spinal cord injury. Since expression of RAG1 encoding gene was not observed under these conditions, DRG cells were cultivated in the presence of secretome of lesion segment from 1 day SCI following by RT-PCR. RT+ : the cDNA was synthetized, RT- : the reverse transcriptase was omitted, H20: negative control.

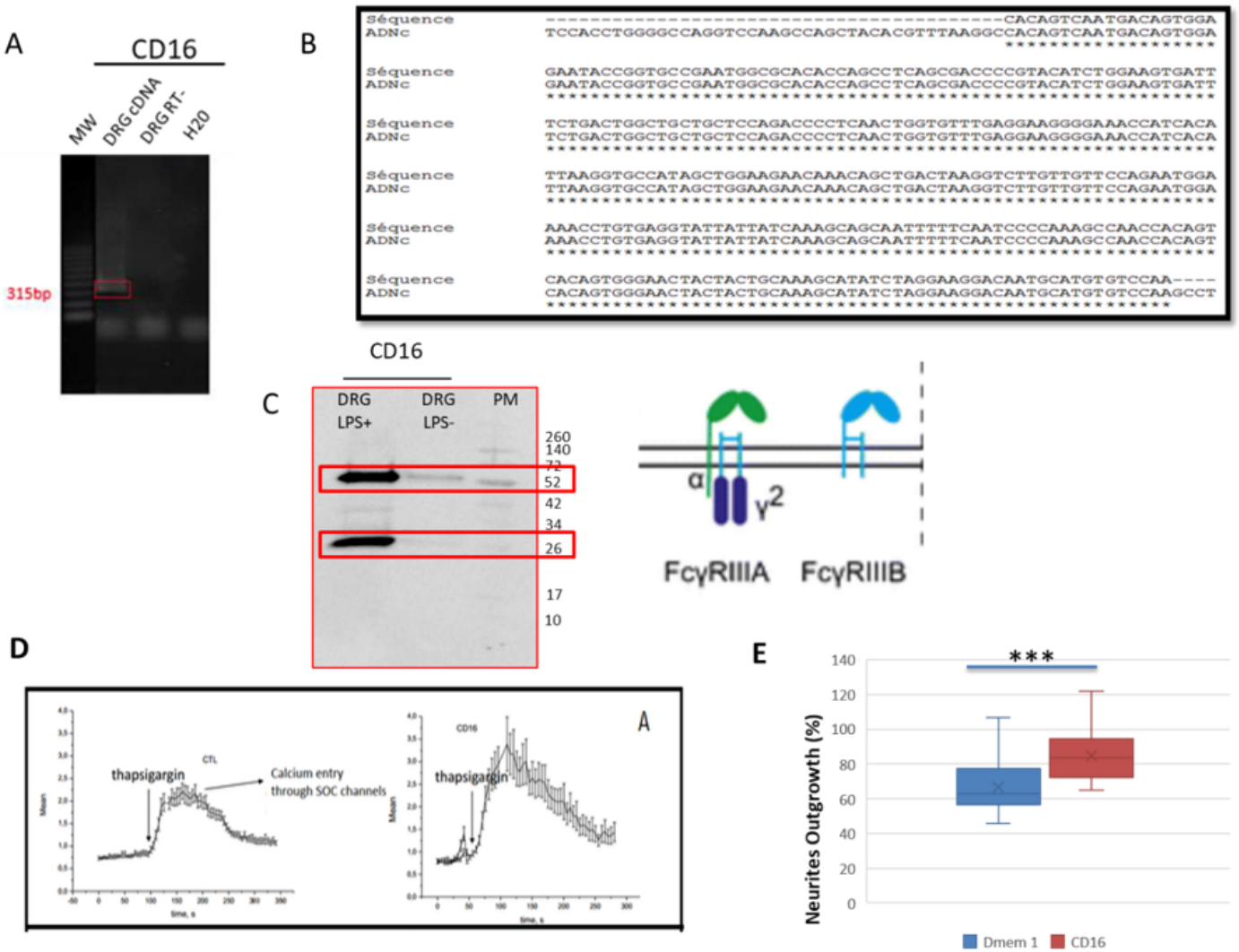

Figure 6

FcgRIII receptors identification in sensory neurons **A**) PCR amplification of the mRNA encoding CD16 receptor. **B**) Sequence alignments of the nucleic acid sequence. **C**) Western blot analysis of DRG cells in presence of LPS treatment or not. **D**) CD16 blocking by specific antibody in TG-activated SOCE conditions impacts Ca^{2+} homeostasis. Quantification of the results are presented in the left panel for the controls and in right panel for CD16 blockage. **E**) DRG ND7/23 neurites outgrowth in presence of specific blocking antibodies directed against CD16 with or without anti-GFAP Mouse anti-GFAP displayed an IgG2 isotype and served as a control of Fc gamma receptors activation.

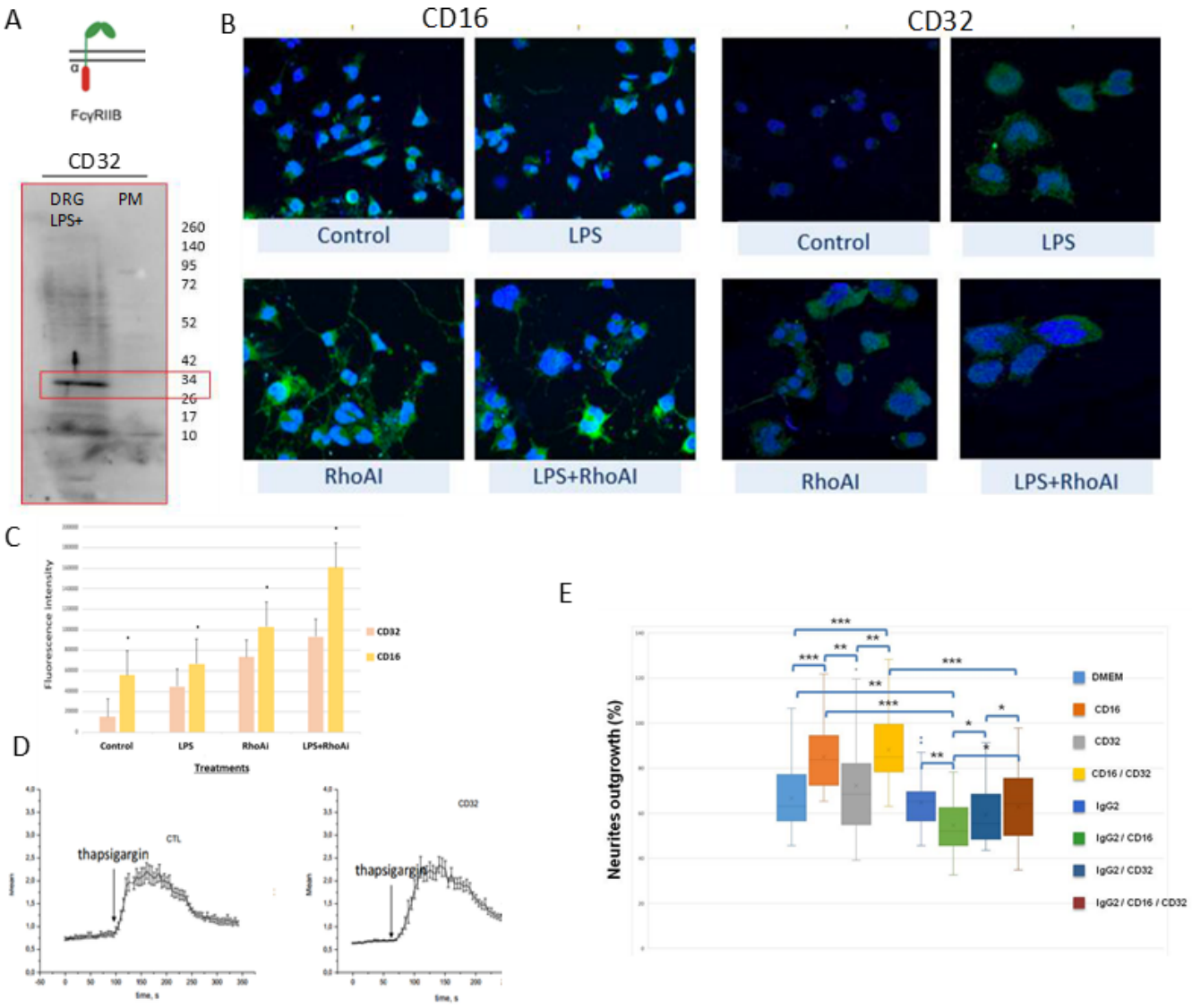

Figure 7

FcgRIIB receptor identification in sensory neurons **A**) Western blot revealing CD32b receptor in DRG cells. **B**) Immunofluorescence performed with anti-CD16 or anti-CD32 on DRG cells stimulated or not with LPS and/or RhoAi. Nuclei were counterstained with DAPI (blue). **C**) Quantification of CD16 and CD32b

immunofluorescence in DRG ND7/23cells after RhoAi and/or LPS treatments.**D**) CD32b blocking by specific antibody in TG-activated SOCE conditions does not impact Ca^{2+} homeostasis. Quantification of the results are presented in the left panel for the controls and in right panel for CD16 blockage. **E**) DRG ND7/23 neurites outgrowth in presence of specific blocking antibodies directed against CD16 or CD32b or CD16and CD32b with or without anti-GFAP Mouse anti-GFAP displayed an IgG2 isotype and served as a control of Fc gamma receptors activation.

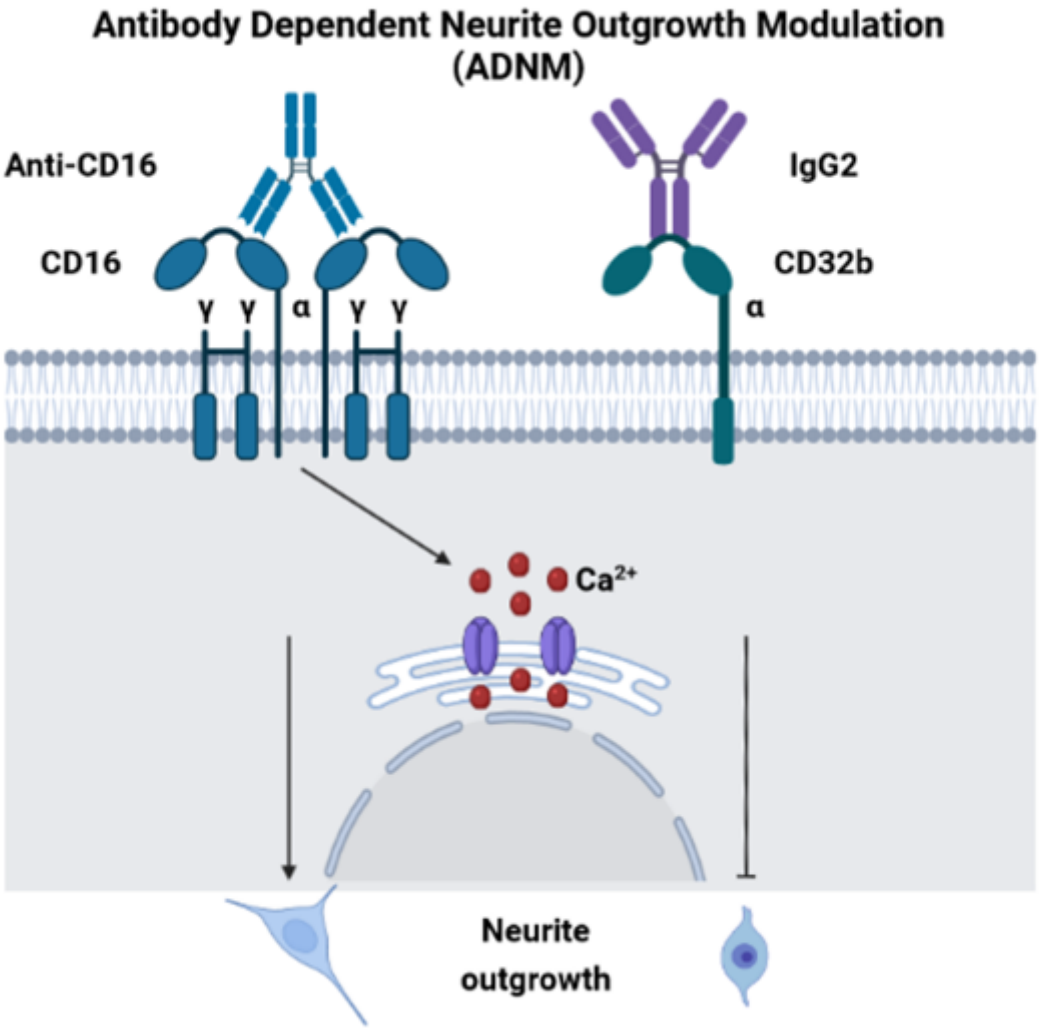

Figure 8

Antibody Dependent Neurite Outgrowth Modulation (ADNM). CD16 activation with anti-CD16 induces calcium release from RE and triggers neurite outgrowth. On the contrary, C32b activation by IgG2 isotype prevents CD16 from triggering neurite outgrowth.

Supplementary Files

This is a list of supplementary files associated with this preprint. Click to download.

- Supp.Data1.xlsx
- Supp.data2.xlsx
- Supp.data3.xlsx
- Supp.data4.zip
- Supp.Data5.xlsx
- Tables.docx
- SupplementaryFile.docx